Inorganic Chemistry

Article

pubs.acs.org/IC

Novel Gold(I) Thiolate Derivatives Synergistic with 5-Fluorouracil as Potential Selective Anticancer Agents in Colon Cancer

Elena Atrián-Blasco,[†,‡] Sonia Gascón,[⊥] Mª Jesus Rodríguez-Yoldi,[⊥] Mariano Laguna,*[,†] and Elena Cerrada*[,†]

[†]Departamento de Química Inorgánica, Instituto de Síntesis Química y Catálisis Homogénea, Universidad de Zaragoza, CSIC, 50009 Zaragoza, Spain

[‡]Laboratoire de Chimie de Coordination (LCC), UPS, INPT, LCC, 205 Route de Narbonne et Universite de Toulouse, F-31077 Toulouse, France

[⊥]Departamento de Farmacología y Fisiología, Unidad de Fisiología, Facultad de Veterinaria, Ciber de Fisiopatología de la Obesidad y Nutrición, Instituto Agroalimentario de Aragón and Instituto de Investigación Sanitaria de Aragón, 50013 Zaragoza, Spain

Supporting Information

ABSTRACT: New gold(I) thiolate complexes have been synthesized and characterized, and their physicochemical properties and anticancer activity have been tested. The coordination of PTA derivatives provides optimal hydrophilicity/lipophilicity properties to the complexes, which present high solution stability. Moreover, the complexes show a high anticancer activity against Caco-2 cells, comparable to that of auranofin, and a very low cytotoxic activity against enterocyte-like differentiated cells. Their activity has been shown to produce cell death by apoptosis and arrest of the cell cycle because of interaction with the reductase enzymes and consequent reactive oxygen species production. Some of these new complexes are also able to decrease the necessary dose of 5-fluorouracil, a drug used for the treatment of colon cancer, by a synergistic mechanism.

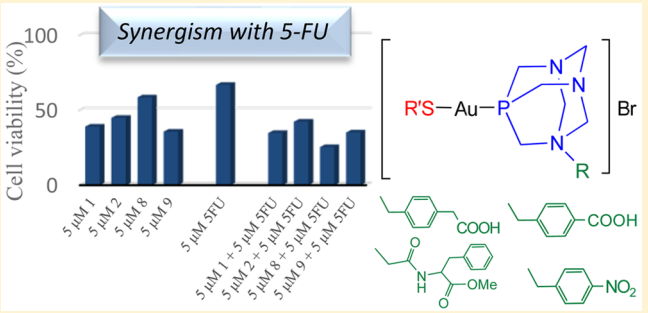

1. INTRODUCTION

Colorectal cancer is one of the most commonly diagnosed cancers. It is the third most common cancer worldwide and the second most common cancer in Europe, according to the GLOBOCAN estimates.[1] The use of [(1*R*,2*R*)-cyclohexane-1,2-diamine](ethanedioato-*O*,*O*′)platinum(II) (oxaliplatin) in adjuvant chemotherapy, in combination with fluorouracil (FU) and leucovorin (LV) or capecitabine, is a standard of care for colon cancer patients in stage III.[2,3] However, this therapy in stage II patients is still controversial.[4,5] Oxaliplatin, a third-generation platinum drug, was the first drug approved that was capable of overcoming cisplatin resistance through the different adducts that form with DNA.[6] Oxaliplatin, like cisplatin, undergoes aquation as a previous step in the formation of a complex with DNA and blocks DNA replication and transcription, primarily by causing intrastrand cross-links in DNA,[7] ultimately triggering cancer cell death. Although the addition of oxaliplatin in the adjuvant chemotherapy has improved the survival of the patients, the incidence of neurotoxicity has increased[8,9] similar to that found in cisplatin-based treatment. The presence of these severe side effects limits the administration dose, thereby reducing the effectiveness of these platinum-based drugs.

To overcome these drawbacks, new metallic compounds have been investigated as potential anticancer drugs. In the particular case of gold, the interest in this metal began with the discovery that patients treated with auranofin for rheumatoid arthritis showed unexpectedly lower malignancy rates.[10] Auranofin has been shown to inhibit the growth of cultured cancer cells in vitro, although a limited activity in vivo.[11] In recent years, the identification of novel mechanisms of action of this gold thiolate derivative has allowed researchers to discover potential new applications that comprise the treatment of various diseases, including several types of leukemia, carcinomas, and parasitic, bacterial, and viral infections.[12] A large variety of gold complexes that show antiproliferative properties against a huge range of cancerous cells have been described in the literature.[13−18] Phosphanegold(I) thiolate derivatives constitute a family of very promising experimental agents for cancer treatment.[19−27] In addition, it has been demonstrated that the presence of a P−Au−S motif increases the anticancer activity compared to thiolates of the type [Au(SR)], thus suggesting a relevant role for the phosphane molecule.[28,29]

Received: May 29, 2017
Published: July 6, 2017

DOI: 10.1021/acs.inorgchem.7b01370
Inorg. Chem. 2017, 56, 8562−8579

The specific mechanism of action of these cytotoxic gold derivatives is still basically unknown, although it seems to be different from those observed in established anticancer drugs, like platinum-based derivatives. Some studies indicate that the main target for gold complexes are selenocysteine (Sec)-dependent enzymes, such as glutathione peroxidase (GPx) and thioredoxin reductase (TrxR).[30−33] As an example, auranofin is reported to strongly inhibit TrxR and thioredoxin glutathione reductase; however, only a modest inhibitory effect is found on glutathione reductase (GR).[34,35] This fact is attributable to the higher affinity of the gold atom to the Sec residue than the cysteine in the protein. The thioredoxin system is being considered as an appropriate target for the development of new anticancer drugs because an overexpression of thioredoxin and TrxR has been found as characteristic in many primary cancers[36] and associated with aggressive tumor growth.[37] Inhibition of the TrxR activity can destroy the redox homeostasis of cells by raising the reactive oxygen species (ROS) levels,[38,39] further leading to cell death by apoptosis or necrosis induction. In fact, the possibility of targeting the redox balance in cancer cells has been recently discussed as a highly effective strategy in cancer treatment because it is considered as a multiple-site approach that offers selectivity toward normal cells.[40]

The choice of ligands in the coordination sphere of the metallic center is crucial, in order to confer specific properties such as stability, lipophilicity, and hydrophilicity. In recent papers, we have reported that the use of water-soluble phosphanes of the type 1,3,5-triaza-7-phosphaadamantane (PTA) and their N-alkylated derivatives has led to water-soluble gold(I) derivatives with antitumor properties against ovarian and/or colon cancer cells (Chart 1). The coordination

Chart 1. Structures of Previously Synthesized and Tested Gold(I) Complexes

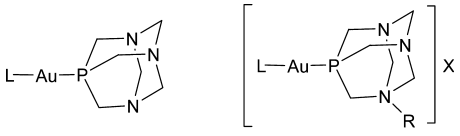

L = Cl, Br, C_6F_5, Spy, Spyrim, SMePyrim, SMe_2pyrim

R = CH_2Ph, $CH_2C{\equiv}CH$, CH_2CO_2Me

of thiolate moieties (pyridine-2-thiol or pyrimidine-2-thiol) has improved the above properties, which include a balanced relationship between the lipophilicity and hydrophilicity and the corresponding antiproliferative behavior.[23,25,26,41−43]

In a previous study, we described the synthesis of gold(I) chloro-, pentafluorophenyl-, and thiocyanate derivatives with N-alkylated PTA molecules incorporating para-substituted benzenes: $-CH_2$-*p*-COOH-C_6H_4, $-CH_2$-*p*-CH_2COOH-C_6H_4, and $-CH_2$-*p*-NO_2-C_6H_4.[44] These residues of the phosphane molecule have been chosen in order to optimize the equilibrium of hydrophilicity/lipophilicity without losing water solubility. Also, the introduction of an acid group could be used for future reactions with amines to get amide moieties. In these derivatives, poor stabilities and low anticancer activities were found; for this reason, here we demonstrate that the replacement of the halogen or pseudohalogen ligands by a thiolate anion improves their stability and biological activity. In addition, preliminary studies on their cytotoxicity against colon cancer have been conducted including synergism/antagonism studies with 5-FU of some of the new complexes. We also include studies concerning the capacity of these compounds to induce apoptosis, their implication in cell cycle progression, and their interaction with BSA, ROS production, and interaction with reductase systems, with the aim of knowing more information about their mechanism of action.

2. RESULTS AND DISCUSSION

2.1. Synthesis and Characterization. Gold(I) thiolate derivatives are usually prepared through the addition of a chlorogold complex to the corresponding thiolate salt prepared in situ by its deprotonation in basic media. However, this method led to mixtures of products when alkylated PTA molecules are coordinated to the metallic center, as a consequence of side reactions of the residue linked to the nitrogen atom of the PTA in the basic conditions. As an alternative, we have recently described the use of tin(IV) thiolate complexes as transmetalating reagents, giving rise to the isolation of pure thiolate derivatives.[23] In order to avoid the additional preparation of these tin compounds, here we have performed the in situ preparation of the corresponding insoluble oligomeric or polymeric $[\{Au(thiolate)\}_n]$, similar to those previously described by Puddephatt et al.[45] Thus, deprotonation of pyridine-2-thiol or pyrimidine-2-thiol with sodium ethoxide (NaOEt) and the subsequent addition of [AuCl(tht)] (tht = tetrahydrothiophene) under an argon atmosphere allows the formation of a solid with the general formula $[\{Au(SR')\}_n]$. The subproducts of the reaction, NaCl and tht, are removed by decantation of the supernatant because the polymer is insoluble in ethanol. The following addition of the alkylated PTA phosphanes [PTA-R]Br in acetone affords the new thiolate derivatives [Au(PTA-R)(SR′)]Br (**1**−**13**; Scheme 1).

The signals corresponding to the thiolate ligands can be seen in the region of 6−8 ppm in their ^{1}H NMR spectra (see the Supporting Information for details). The signals of the phosphane fragment are very similar to those observed in the previously reported gold chloro-, pentafluorophenyl-, or isothiocyanate complexes [AuL(PTA-R)]X.[44] Thus, a broadening of the signals is observed, and the methylene protons of the PTA fragment appear shifted to lower field in comparison to the free phosphanes. Broad singlets, downfield displaced compared with the signals of free phosphanes, are detected in their ^{31}P{^{1}H} NMR spectra. Broadening of the signals in the NMR spectra could indicate the presence of an ionic interchange of the thiolate ligand and the bromide. This fact is supported by the appearance of a peak corresponding to such an ion exchange, $[M(SR')+Br]^+$, in the positive-ion matrix-assisted laser desorption/ionization ($MALDI^+$), which is seen for complexes [Au(SMepyrim)(PTA-CH_2-*p*-COOH-C_6H_4)]Br (**3**), [Au(SMepyrim)(PTA-CH_2-*p*-CH_2COOH-C_6H_4)]Br (**7**), and [Au(Spyrim)(PTA-CH_2-*p*-NO_2-C_6H_4)]Br (**10**) with a relative abundance higher than 10% and for complexes [Au(Spyrim)(PTA-CH_2-*p*-COOH-C_6H_4)]Br (**2**), [Au(SMe_2pyrim)(PTA-CH_2-*p*-COOH-C_6H_4)]Br (**4**), [Au(Spy)(PTA-CH_2COOH-C_6H_4]Br (**5**), and [Au(SMepyrim)(PTA-CH_2-*p*-NO_2-C_6H_4)]Br (**11**) with a relative abundance lower than 10%.

2.2. Physicochemical Properties. *2.2.1. Lipophilicity.* There is a recent discussion about the importance of optimizing the absorption, metabolism, excretion, and toxicity (ADME/Tox) properties of derivatives to increase drug-discovery

DOI: 10.1021/acs.inorgchem.7b01370
Inorg. Chem. 2017, 56, 8562−8579

Scheme 1. Preparation of Phosphanegold(I) Thiolate Derivatives[a]

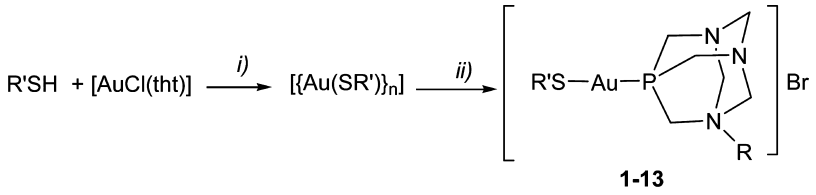

1-13

R \ SR'				
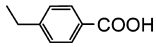	1	2	3	4
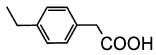	5	6	7	8
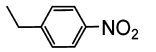	9	10	11	12
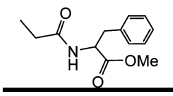	13			

[a](i) NaOEt; (ii) [PTA-R]Br.

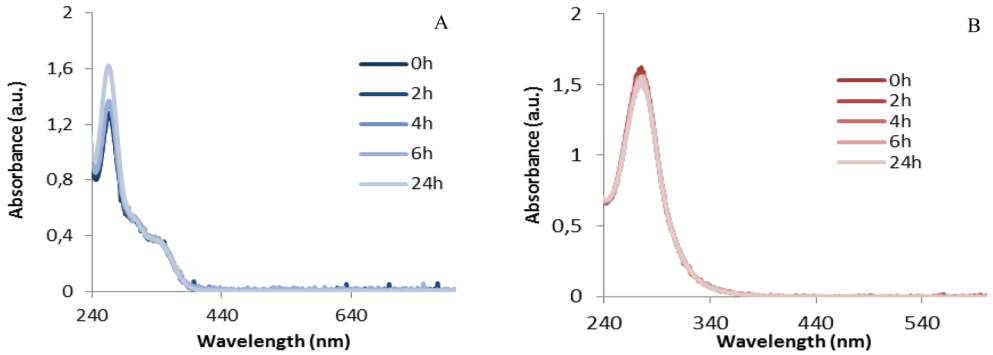

Figure 1. UV−vis spectra of (A) **5** and (B) **10** for a period of 24 h.

success.[46] Properties such as the solubility, permeability, and stability are recognized to have an important effect on the performance of drug research. Lipophilicity is a property with a high impact on the ADME/Tox properties and has been correlated to other properties such as solubility, permeability, metabolism, toxicity, protein binding, and distribution. The lipophilicity of a compound is directly related to its diffusion and permeation into the lipid bilayer membrane of the cells, thus affecting not only its activity but also its toxicity toward healthy tissues. Furthermore, it is directly related to the plasma protein binding and metabolism of the drug.[47] Lipophilicity, or, more appropriately, the balance between the lipophilicity and hydrophilicity, can be measured by the partition coefficient water/octanol, log P (for neutral complexes) or log D_{pH} (for ionizable molecules).

Measurement of the distribution coefficient of a molecule can be done by experimental procedures such as the shake-flask method, which studies the distribution of the drug between an equal amount of octanol and water (or a buffered aqueous solution). The physicochemical similarity of 1-octanol to lipids makes it the most appropriate hydrophobic solvent. Changes in the drug lipophilicity have been shown to have a great impact on the antitumor activity and host toxicity; thus, many authors have tuned the hydrophilic/lipophilic properties of molecules by the incorporation of appropriate functional groups to optimize the activity and reduce the toxicity.[48−50] In addition, previous studies on phosphanegold(I) derivatives[51] have revealed the impact of high lipophilicity on the host toxicity, resulting in drug accumulation in the mitochondria.[52] Consequently, a balanced relationship between the lipophilicity and hydrophilicity would be important in a drug-delivery process. The hydrophilicity/lipophilicity balance has been optimized by changing the ligands or functionalizing the PTA moiety in the complexes synthesized by our research group.[23,42,44,53,54] In this context, the use of modified PTA molecules with acidic, nitro, and biomimetic amino acid moieties gives values of log $D_{7.4}$ (see the Experimental Section for details) in the range −0.8 to +1.2 (Table 3). The nature of the phosphane seems to have a great influence; consequently, similar values are obtained with the same phosphanes. Thus,

DOI: 10.1021/acs.inorgchem.7b01370
Inorg. Chem. 2017, 56, 8562−8579

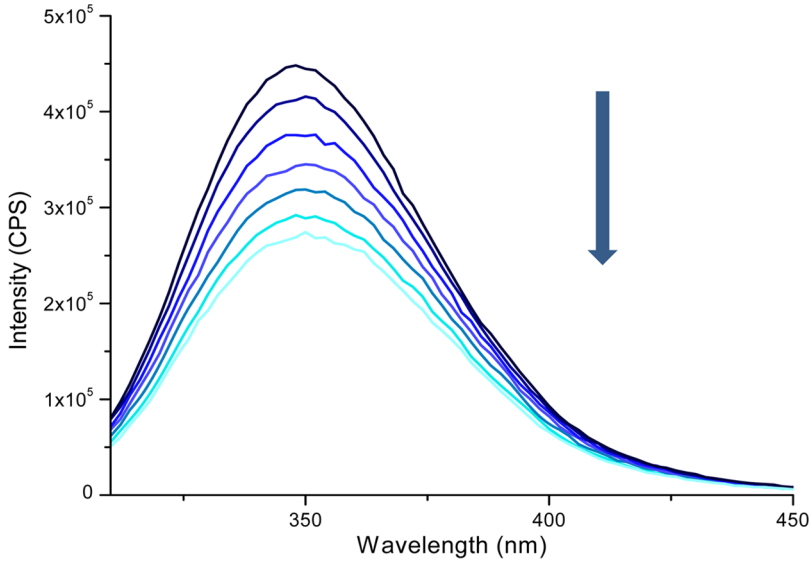

Figure 2. Fluorescence emission spectra of BSA at 298 K in the presence of different concentrations of **1**. The arrow indicates the increase of the quencher concentration (0−30 μM).

the compounds with phosphanes [PTA-CH_2-*p*-COOH-C_6H_4]Br and [PTA-CH_2-*p*-CH_2COOH-C_6H_4]Br are more hydrophilic (i.e., their log $D_{7.4}$ < 0) than the complexes with [PTA-CH_2-*p*-NO_2-C_6H_4]Br and [PTA-CH_2CONHCH(CH_2Ph)-COOMe]Br (log $D_{7.4}$ > 0). These data are in agreement with their water solubility. Thus, the most soluble derivatives display negative log $D_{7.4}$ values, as expected for more hydrophilic substances. Likewise, according to the established relationship between the solubility and drug likeness by Cheng and Merz,[55] all of the new thiolate complexes described here are in the range from good to optimal drug likeness (−4 < log S_w < 0, where S_w = solubility value in mol L^{-1}).

2.2.2. Solution Stability. Stability of a complex in solution is necessary for success in the development of a successful drug product.[56,57] A potential anticancer drug must be stable in biological assay buffers in order to produce accurate activity in enzyme, receptor, and cell-based assays. The compound should not undergo any reaction with oxygen, water, or the excipients present in the solution, which could compromise its activity.

We have studied the solution stability of the new complexes under physiological conditions, by dissolving them in phosphate-buffered saline (PBS) at pH 7.4 and maintained at 37 °C. The UV−vis absorption spectrum of each complex was recorded at different time intervals. Through a comparison of the spectra obtained at every time, it was possible to qualitatively determine the stability of the compounds under such conditions (see Figure 1 as an example and Figure S50). Complexes with the phosphane [PTA-CH_2-*p*-NO_2-C_6H_4]Br seem to be the most stable. In all of them, a single band at 270 nm is observed and can be assigned to the nitrobenzene residue and maintained unchanged over time. Complexes with acidic moieties in the phosphane molecule, [PTA-CH_2-*p*-COOH-C_6H_4]Br and [PTA-CH_2-*p*-CH_2COOH-C_6H_4]Br, have similar behavior: their UV−vis spectra show intense bands in the range between 265 and 300 nm, which can be assigned to aromatic transitions. In the case of complexes [Au(Spy)(PTA-CH_2-*p*-COOH-C_6H_4)]Br (**1**) and **5**, additional bands appeared, characteristic of the gold(I) chromophore, that could be assigned as metal-to-ligand charge-transfer bands.[58] In general, an increase of the intensity of the band is observed that does not seem to affect the general stability of these complexes nor their activity. In general, these thiolate derivatives are more stable and display higher cytotoxicity (see below) than the previously reported gold(I) chloro-, pentafluoro-, and isothiocyanate complexes.[44] Consequently, changing the ligand from a halogen or pseudohalogen to thiolate seems to be a good strategy to increase the stability under physiological conditions, which leads to an improvement of their effectiveness as anticancer drugs.

Additional stability studies were performed by NMR experiments over a 24 h period after dilution of deuterated dimethyl sulfoxide (DMSO-d_6) solutions of the complexes with a PBS solution (pH 7.4). Complexes with the acid moiety in the PTA molecule show new emerging signals in the aromatic region, which increase over time in their ^{1}H NMR spectra (see the spectra recorded in the Supporting Information). The same pattern is observed in the new signals in all cases, which is consistent with the presence of para-substituted benzene units (AA′XX′ system). This feature is not observed in **11**, whose ^{1}H NMR spectrum remains unchanged in the hydrolysis experiment. The rest of the complexes with [(PTA-CH_2-*p*-NO_2-C_6H_4)]Br phosphane displayed lower solubility in the buffered solution, and some of them precipitated during the NMR measurements. Besides, new signals are also observed in the ^{31}P{^{1}H} NMR spectra of complexes **1**−**7**, and no release of the phosphane is detected. Conversely, related thiolate derivatives with alkylated PTA molecules described by some of us[23] proceeded with phosphane dissociation and subsequent oxidation after dissolution in a buffered water solution, similar to that found in auranofin.[59] These findings suggest the occurrence of hydrolysis reactions under buffer conditions for complexes with −COOH moieties. However, the presence of nitro substituents in the para position leads to higher stability of the corresponding compounds under the same conditions, which is in agreement with the results observed in the UV−vis absorption studies.

2.2.3. Bovine Serum Albumin (BSA) Interaction. Most chemotherapeutic treatments use the bloodstream to deliver the drug to the target, where there are a variety of blood constituents, such as plasma proteins, capable of interacting

DOI: 10.1021/acs.inorgchem.7b01370
Inorg. Chem. 2017, 56, 8562−8579

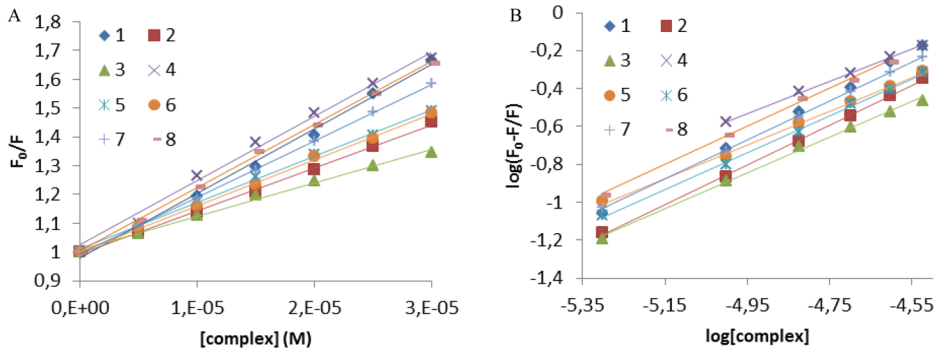

Figure 3. (A) Stern−Volmer plot for BSA fluorescence quenching observed for complexes **1**−**8**. (B) Representation of the modified Stern−Volmer plot.

with the drug. Thus, plasma protein binding can influence the important properties of a drug such as its absorption and distribution, having an impact on the pharmacokinetic and pharmacodynamics profiles of the compound as well as its dosing regimen. For this reason, the study of plasma protein binding is an important part of the determination of the Administration/Absorption, Distribution, Metabolism, Excretion (ADMET) properties of our new compounds. Albumin (HSA in humans), which is the most abundant plasma protein, contains 585 amino acids and two main binding sites I and II,[60] where substances are from weakly to tightly bonded by hydrophobic interactions.

In fact, the primary functions of HSA include the transport of molecules through the body in addition to the blood pH and osmotic pressure maintenance. Studies of albumin binding of antiarthritic gold complexes such as auranofin have revealed that the residue Cys-34 is the main binding site for gold(I) in albumin.[61,62]

It seems that low protein binding appears to be advantageous because some authors have indicated that a high affinity toward protein thiols limits the anticancer in vivo activity of gold(I) anticancer complexes compared to their in vitro activity.[63] BSA is frequently used as a model protein for HSA because of their similarity, with a homology of ca. 76%, and some concerns about the heterogeneity of commercially available samples of HSA.[64] BSA possesses three fluorophores: two tryptophan residues—Trp134, found on the surface of the protein, and Trp212, located in a hydrophobic binding pocket—and tyrosine and phenylalanine residues, which do not seem to have an important contribution, inasmuch as the emission intensity of the tryptophan residues is approximately 5 times greater.[65] The intrinsic fluorescence of BSA is sensitive to its local environment, and binding or simple electrostatic interaction of molecules can produce changes in its emission spectrum. The addition of increasing amounts of thiolate derivatives to a solution of BSA resulted in a quenching of its fluorescence emission upon excitation at 295 nm (Figures 2 and S55). The fluorescence of the tested gold(I) thiolate complexes was measured under the same experimental conditions, and no emission was observed in the range 310−450 nm.

The quenching of the emission intensity has been produced without an observable change of either the shape of the band or the maximum of the emission. The fluorescence data have been analyzed using the Stern−Volmer equation (see the Experimental Section) so the binding of the complexes to BSA and the consequent quenching of the emission can be quantified by a representation of the plot F_0/F versus [complex] (F_0 = intensity in the absence of the quencher; F = intensity in the presence of the quencher; Figure 3 and Table 1). All of the quenching constant values (K_{SV} and k_q) remain on the same order of magnitude for all of the complexes.

Table 1. Values of the Stern−Volmer Quenching Constant (K_{SV}), Bimolecular Quenching Constant (K_q), Apparent Binding Constant (K_b), and Number of Binding Sites (n) for the Interaction of Complexes 1−8 with BSA

compound	$K_{SV} \times 10^4$ (M^{-1})	$k_q \times 10^{12}$ (M^{-1} s^{-1})	K_b (M^{-1})	n
[Au(Spy)(PTA-CH_2-*p*-COOH-C_6H_4)]Br (**1**)	3.44	3.44	1.50×10^4	1.17(1)
[Au(Spyrim)(PTA-CH_2-*p*-COOH-C_6H_4)]Br (**2**)	1.50	1.50	2.40×10^4	1.05(1)
[Au(SMepyrim)(PTA-CH_2-*p*-COOH-C_6H_4)]Br (**3**)	1.16	1.16	6.76×10^3	0.95(1)
[Au(SMe_2pyrim)(PTA-CH_2-*p*-COOH-C_6H_4)]Br (**4**)	2.24	2.24	4.82×10^3	0.85(1)
[Au(Spy)(PTA-CH_2-*p*-CH_2COOH-C_6H_4)]Br (**5**)	1.78	1.78	3.61×10^2	0.89(1)
[Au(Spyrim)(PTA-CH_2-*p*-CH_2COOH-C_6H_4)]Br (**6**)	1.60	1.60	1.23×10^4	0.98(1)
[Au(SMepyrim)(PTA-CH_2-*p*-CH_2COOH-C_6H_4)]Br (**7**)	1.96	1.96	2.55×10^4	1.03(1)
[Au(SMe_2pyrim)(PTA-CH_2-*p*-CH_2COOH-C_6H_4)]Br (**8**)	2.19	2.19	2.12×10^4	1.00(1)

In all of the cases studied, the Stern−Volmer representation (Figure 3A) fits a straight line, indicative of a single quenching mode, either static or dynamic. Dynamic quenching is caused by diffusion and static quenching by ground-state complex formation.[66] Several methods can be used to determine which quenching mechanism, either dynamic or static, is predominant for each experiment, based on their physical properties.[66] Dynamic and static quenching can be distinguished by a study of the bimolecular quenching constant, k_q. This constant represents the efficiency of quenching or how accessible the fluorophores are to the quencher. Because dynamic quenching depends on diffusion, a k_q value higher than the diffusion-controlled rate constant of the biomolecule in water, 10^{10} M^{-1} s^{-1}, could indicate some type of binding interaction, implying a possible contribution of static quenching. In our case, the values of k_q are on the order of 1×10^{12} M^{-1} s^{-1}, so binding of the complexes and BSA could be considered. Examination of the absorption spectra of the fluorophores can also be useful in characterizing static and dynamic quenching.

DOI: 10.1021/acs.inorgchem.7b01370
Inorg. Chem. 2017, 56, 8562−8579

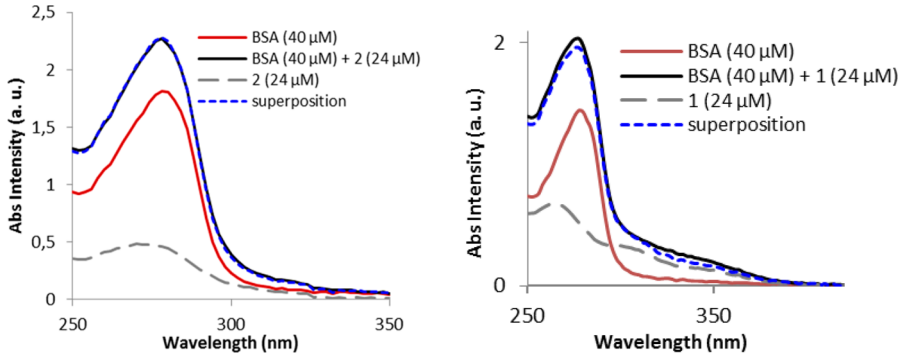

Figure 4. Absorption spectra of BSA (red solid line), compounds **1** and **2** (dashed gray line), BSA + compound (black solid line), and their superposition (dotted blue line).

Given the idea that static quenching implies complex formation, changes in the absorption spectra of BSA could be expected, while dynamic quenching only affects the excited states of BSA and its absorption spectra would remain unchanged (Figure 4).

The absorption spectra of BSA in the absence and presence of each one of the compounds in a concentration of 24 μM, as well as the absorption spectrum of the compound at the same concentration, were recorded. A mathematical superposition of the spectrum of BSA and that of the compounds was calculated. In most of the cases, the addition of both spectra can be superposed to the spectrum of BSA + complex, implying dynamic binding. However, in some cases as with complexes **1** and **5**, there is a slight deviation in the superposition; therefore, both dynamic and static binding modes could be implied.

Dynamic and static quenching can also be distinguished by their temperature dependence. Thus, the dynamic mechanism depends on diffusion and increases with the temperature. Consequently, the quenching constant K_{SV} is expected to increase with the temperature. Table 2 displays the values of

Table 2. Values of the Quenching Constant (K_{SV}) for BSA Interaction with Complexes 1 and 5 at Different Temperatures

compound	T (K)	K_{SV} (M^{-1})	compound	T (K)	K_{SV}(M^{-1})
1	299	3444.8	**5**	299	1788.5
	304	3415.4		304	1217.1
	310	2788.2		310	862.32

K_{SV} at three temperatures for complexes **1** and **5**. The results indicate that the Stern−Volmer quenching constant is inversely correlated with the temperature in both cases, which is in agreement with the formation of a complex of the quencher with BSA (static mechanism).

Representation of $\log(F_0 - F/F)$ versus log [complex] (Figure 3B) has allowed us to calculate the values of the binding constant for each experiment and the number of binding sites, summarized in Table 1. The binding constant values range from 3.6×10^2 to 2.5×10^4 M^{-1}. These values are in agreement with those observed for gold(III) derivatives,[67] the gold(I) cyanide complex[68] $[Au(CN)_2]^-$, or in gold(I) alkyne complexes described by us.[69] However, they are slightly bigger than the binding constant of cisplatin[70] with HSA, which was found to be 8.52×10^2 M^{-1}. The values of the binding constant of gold nanoparticles[71,72] are generally much greater, of about 10^{10} M^{-1}. In our case, moderate BSA binding is observed, which makes the complexes suitable candidates for in vivo experiments. There are no clear differences between the different families of complexes depending on the phosphane or the thiolate ligand.

2.3. Biological Studies. The antiproliferative effects of the new thiolate complexes were evaluated against two different clones of the cancerous cell line Caco-2 (PD7 and PC7). The colon cancer cell line Caco-2 was established by Jorgen Fogh from a human colon adenocarcinoma. Caco-2 cells can develop a spontaneous and homogeneous enterocytic differentiation upon reaching confluence for 21 days to become polarized cells expressing apical and basolateral surfaces with well-established tight junctions.[73,74] Both clones, PD7 and TC7, show high rates of glucose consumption and similar functionalities[75] but with a difference in their origin: PD7 preceded from early passages, thus making them more heterogeneous, and TC7 from late passages, presenting higher stability and homogeneity. Cultured cancer cells were treated with increasing concentrations of gold derivatives for 72 h, and the corresponding IC_{50} values (Table 3) were determined by using the MTT protocol.[76] All of the complexes show a better anticancer activity (IC_{50} values ranging from 2.00 to 13.37 μM) than the previously reported chloro- and thiocyanate gold homologues,[44] better also than the reference drug cisplatin and in the same range, in most of the cases, than those measured for auranofin. Comparing the activity of the complexes depending on the nature of the phosphane, the best results are obtained in the case of the $[PTA\text{-}CH_2\text{-}p\text{-}COOH\text{-}C_6H_4]Br$ molecule and $[PTA\text{-}CH_2\text{-}p\text{-}NO_2\text{-}C_6H_4]Br$, with the lowest IC_{50} concentrations. Although a pattern of activity cannot be established for the different thiolate ligands, we can say that complexes bearing thiolpyridine and the phosphanes $[PTA\text{-}CH_2\text{-}p\text{-}COOH\text{-}C_6H_4]Br$ and $[PTA\text{-}CH_2\text{-}p\text{-}NO_2\text{-}C_6H_4]Br$ (**1** and **9**, respectively) have the lowest IC_{50} values against both clones PD7 and TC7, while the compounds with the same thiolate ligand and the phosphane $[PTA\text{-}CH_2\text{-}p\text{-}CH_2COOH\text{-}C_6H_4]Br$ have an IC_{50} concentration of approximately double the value. All of the complexes display higher cytotoxicity than the previously described chloro- and pseudohalogen gold(I) complexes with the same PTA phosphanes.[44] This observed improvement in the activity could be related to a greater stability in a solution of the here-described thiolate complexes compared to the pseudohalogen ones. In fact, a reduction to metallic gold could be observed in some cases for the previously published complexes[44] (data not shown/published) after 12 h in solution, which could limit their effectiveness in in vitro toxicity studies. This is not the case for the thiolate complexes described here. Some preliminary

DOI: 10.1021/acs.inorgchem.7b01370
Inorg. Chem. 2017, 56, 8562−8579

Table 3. IC_{50} Values and Distribution Coefficients of the Thiolate Complexes against Caco-2/PD7 and Caco-2/TC7 Colon Cancer Cell Lines Compared with Auranofin and Cisplatin

compound	log $D_{7.4}$	IC_{50} (μM)[a]	
		PD7	TC7
[Au(Spy)(PTA-CH_2-*p*-COOH-C_6H_4)]Br (**1**)	−0.44	2.00 ± 0.58	2.68 ± 0.30
[Au(Spyrim)(PTA-CH_2-*p*-COOH-C_6H_4)]Br (**2**)	−0.83	2.30 ± 1.02	6.47 ± 2.15
[Au(SMepyrim)(PTA-CH_2-*p*-COOH-C_6H_4)]Br (**3**)	−0.67	2.73 ± 2.08	1.92 ± 1.64
[Au(SMe_2pyrim)(PTA-CH_2-*p*-COOH-C_6H_4)]Br (**4**)	−0.81	6.83 ± 0.50	7.66 ± 0.09
[Au(Spy)(PTA-CH_2-*p*-CH_2COOH-C_6H_4)]Br (**5**)	−0.35	6.99 ± 0.53	4.61 ± 0.14
[Au(Spyrim)(PTA-CH_2-*p*-CH_2COOH-C_6H_4)]Br (**6**)	−0.88	13.37 ± 3.93	10.66 ± 2.56
[Au(SMepyrim)(PTA-CH_2-*p*-CH_2COOH-C_6H_4)]Br (**7**)	−0.26	8.90 ± 1.79	5.06 ± 0.78
[Au(SMe_2pyrim)(PTA-CH_2-*p*-CH_2COOH-C_6H_4)]Br (**8**)	−0.79	5.36 ± 1.95	6.29 ± 1.07
[Au(Spy)(PTA-CH_2-*p*-NO_2-C_6H_4)]Br (**9**)	1.03	2.98 ± 0.83	3.08 ± 0.79
[Au(Spyrim)(PTA-CH_2-*p*-NO_2-C_6H_4)]Br (**10**)	1.24	6.43 ± 1.70	2.98 ± 1.28
[Au(SMepyrim)(PTA-CH_2-*p*-NO_2-C_6H_4)]Br (**11**)	0.74	4.01 ± 1.29	6.08 ± 0.38
[Au(SMe_2pyrim)(PTA-CH_2-*p*-NO_2-C_6H_4)]Br (**12**)	1.2	6.18 ± 0.01	3.96 ± 1.33
[Au(Spy)(PTACH_2CONHCH(CH_2Ph)CO_2Me)]Br (**13**)	0.51	8.36 ± 1.00	6.13 ± 0.92
cisplatin	−0.53	37.24 ± 5.15	45.6 ± 8.08
auranofin	−2.53	1.8 ± 0.1	2.1 ± 0.4

[a]Mean ± SE of at least three determinations.

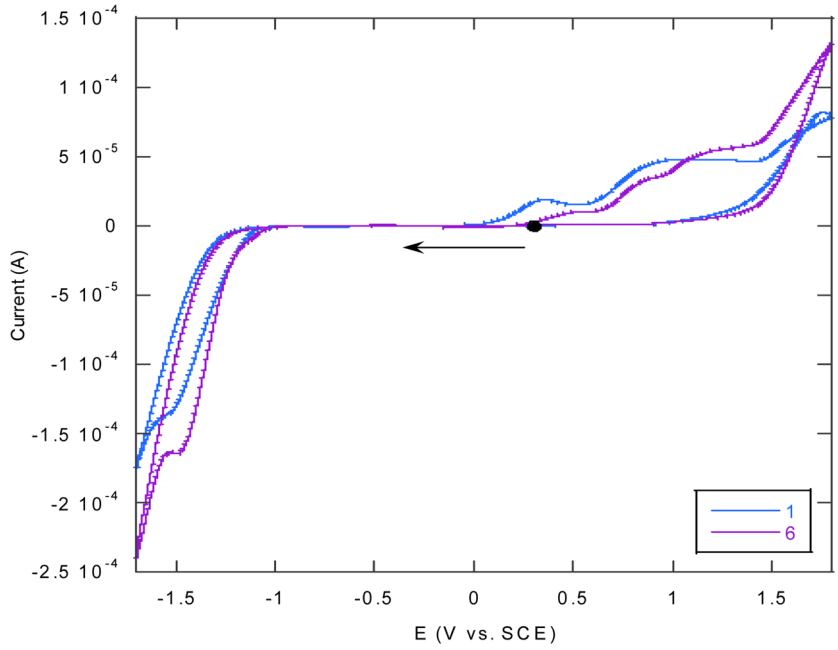

Figure 5. Cyclic voltammograms of complexes **1** (blue line) and **6** (violet line). Starting potential: 0.3 V.

experiments on the reduction of Au^I to Au^0 have been carried out by cyclic voltammetry (CV). As an example, the cyclic voltammograms of the most (**1**) and least (**6**) active (IC_{50}-related) complexes are shown in Figure 5. For both, a cathodic process can be observed at around −1.50 V (vs SCE), related to the reduction of Au^I to Au^0; however, no deposition of metallic gold on the working electrode could be observed, as it has been previously described when using a glassy carbon electrode.[77] The relatively low reduction potentials can be attributed to stabilization of Au^I by the phosphanes. For these complexes, several irreversible anodic features can be observed. As has been described in the case of auranofin,[78] the first anodic peak can be attributed to a sulfur-based oxidation and the second one to the oxidation of Au^I to Au^{III}. Similar values have been obtained for both complexes but seem to be dependent on the nature of the thiolpyridine or thiolpyrimidine used (see Figure S53). We cannot attribute a structure/activity relationship based on these results obtained in the CV experiments.

Comparing the data depicted in Table 3 of the IC_{50} values measured in the previously reported thiolate derivatives with the related alkylated PTA phosphanes shown in Chart 1, we can conclude that the incorporation of electron-withdrawing groups (−COOH and $-NO_2$) in the para position of the phenyl ring barely modifies the anticancer activity because values in similar ranges are obtained in most of the cases. However, there is an important difference in their lipophilic character. Thus, the most electron-withdrawing group ($-NO_2$) gives higher lipophilicity (log *D* values around +1), while the acid group leads to more hydrophilic character (log *D* values ranging from −0.2 to −0.8). Nevertheless, we can compare the complexes by tetrads of the same phosphane. A nonlinear correlation between the lipophilic character of the compounds,

DOI: 10.1021/acs.inorgchem.7b01370
Inorg. Chem. 2017, 56, 8562−8579

by changing the thiol group and their cytotoxic activity, was found. When the lipophilic character is increased, with increasing log *D* values, the activities of the complexes describe an inverted U-shaped curve (Figure 6 as an example and Figure S54), except in the case of derivatives with [PTA-CH_2-*p*-COOH-C_6H_4]Br with Caco2-PD7 cells. According with the observed relationship, the highest anticancer activity should be expected for derivatives with those ligands able to give intermediate log *D* values, namely, around −0.6 for [PTA-CH_2-*p*-COOH-C_6H_4]Br and [PTA-CH_2-*p*-CH_2COOH-C_6H_4]Br phosphanes and around 1 for [PTA-CH_2-*p*-NO_2-C_6H_4]Br phosphane.

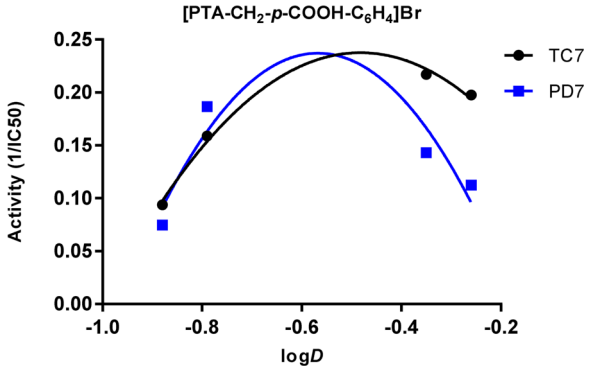

Figure 6. Correlation between the cytotoxic activity of the complexes with [PTA-CH_2-*p*-CH_2COOH-C_6H_4]Br phosphane and log $D_{7.4}$. The activities are calculated as the inverse of IC_{50} in Caco-2/PD7 and Caco-2/TC7. The curves are extrapolated with the *GraphPad Prism* program.

One of the problems found in potential anticancer drugs is their toxicity to healthy tissues caused by a low selectivity toward cancerous cells. Since this toxicity is the source of undesired side effects, it is essential to study the toxicity of a compound to normal cells. Caco-2 cells, upon reaching confluence, form a monolayer of polarized cells, presenting a structure of brush border on the apical surface with tight junctions. This brush border is comparable to the one observed in healthy human small-intestinal tissue, expressing also the same hydrolases, nutrient transporters, bacterial receptors, and other proteins present in enterocytes.[79] Consequently, the toxicity of some of the compounds to the differentiated cells (Caco-2/PD7 cells under confluence) has been tested.

We have chosen those compounds with the pyridine thiolate moiety, which gave the best cytotoxic activity. Thus, treatment of Caco-2/PD7 cells after differentiation with complexes **1**, **5**, [Au(Spy)(PTA-CH_2-*p*-NO_2-C_6H_4)]Br (**9**), and [Au(Spy)-(PTACH_2CONHCH(CH_2Ph)CO_2Me)]Br (**13**) at the corresponding concentrations equivalent to IC_{50} and 2 × IC_{50} values for 72 h gave a percentage of the cell viability next to 100% (Figure S68). Furthermore, the IC_{50} values of these complexes against differentiated Caco-2 PD7 and TC7 cells and their corresponding tumor selectivities were calculated (Table S2). All of the IC_{50} values against differentiated cells are above 30 μM. Moreover, the tumor selectivity is high for all of the complexes, especially in the case of **1** and **9**.

2.4. Combinatory Studies of Gold Complexes with 5-Fluorouracil (5-FU). 5-FU is the most used drug against colorectal cancer, usually in combination with LV and oxaliplatin in an adjuvant treatment known as FOLFOX therapy.[2,80] The combination of oxaliplatin and LV with 5-FU has a synergetic action, improving the activity of 5-FU and overcoming drug-resistance problems. We have studied the synergism/antagonism effect of the coadministration of synthesized gold complexes that have shown good cytotoxic effects against Caco-2/PD7 and TC7 cells with 5-FU [IC_{50}(5-FU) = 20.25 μM for Caco-2/PD7 and 1.89 μM for Caco-2/TC7]. The chosen gold(I) derivatives for the combinatory studies present a variety of low-to-medium IC_{50} values, having different phosphanes and thiolate ligands: [Au(Spy)(PTA-CH_2-*p*-COOH-C_6H_4)]Br **1**, [Au(Spyrim)(PTA-CH_2-*p*-COOH-C_6H_4)]Br **2**, [Au(SMe_2pyrim)(PTA-CH_2-*p*-CH_2COOH-C_6H_4)]Br (**8**), and **9**.

The incubation of Caco-2 cells with gold complexes and 5-FU in a 1:1 molar ratio, with total concentrations of 0, 1.25, 2.5, 5, 10, and 20 μM, gave the IC_{50} values gathered in Table 4.

Table 4. IC_{50} Values (μM) of the Different Combinations

combination	Caco-2/PD7	Caco-2/TC7
c1 (**1** + 5-FU)	3.18	3.25
c2 (**2** + 5-FU)	6.57	9.25
c3 (**8** + 5-FU)	2.06	0.74
c4 (**9** + 5-FU)	3.06	2.95

Only in the case of the combination c3 (**8** + 5-FU), a lower IC_{50} value is obtained compared to both values of **8** and 5-FU on their own in both cell lines (see Table 3). In the case of the combination c4 (**9** + 5-FU), improvement is only observed against the cell line Caco-2/TC7. Most of the gold(I) thiolate derivatives do not show an improvement when combined with 5-FU because their IC_{50} values were already low. On the other hand, the combination improves the effect of 5-FU, especially against the clone PD7. However, considering that the doses are in a 1:1 molar ratio (for 20 μM:10 μM gold(I) thiolate + 10 μM 5-FU), it can be said that, in most of the cases described earlier, there is a reduction in the dose needed for the same effect, as we will analyze later. The effectiveness of the gold(I) thiolate derivatives and 5-FU, alone or in combination, on the inhibition growth of Caco-2 cells has been assessed by measurement of the "combination index" (CI) described by Chou and Talalay in 1984.[81] The CI for different drug combinations has been calculated for different growth inhibition effects: F_a = 0.5, 0.75, 0.9, and 0.95 (see Table 5), using the software *CompuSyn Synergism* (CI < 1) between the gold(I) thiolate complexes and 5-FU, is achieved in ca. 65% of the events. While the combination c2 (**2** + 5-FU) shows the lowest synergistic activity in both cell lines, the combination c3 (**8** + 5-FU) has the most synergic activity for both the PD7 and TC7 cell lines at all growth inhibition effects, and c1 (**1** + 5-FU) is especially synergistic at high growth inhibition effects, when it is more relevant for anticancer therapy.

The main advantage of combining the gold(I) complexes with 5-FU is a reduction of the needed dose for the same effect (Figure 7), expressed by the dose reduction index (DRI; see Table 6), which measures how many folds the dose of each drug in a synergistic combination may be reduced at a given effect level compared to the doses of each drug alone, and is also calculated by *CompuSyn* for a given growth inhibition effect (F_a). The DRI is calculated by the equations

$$(\mathrm{DRI})_{\mathrm{Au}} = \frac{(D)_{\mathrm{Au}}}{(D_{\mathrm{comb}})_{\mathrm{Au}}}; \qquad (\mathrm{DRI})_{\text{5-FU}} = \frac{(D)_{\text{5-FU}}}{(D_{\mathrm{comb}})_{\text{5-FU}}}$$

DOI: 10.1021/acs.inorgchem.7b01370
Inorg. Chem. 2017, 56, 8562−8579

Table 5. CI Values of c1−c4 at Different Inhibition Rates and Cell Lines

	growth inhibition effect (F_a)							
	50%		75%		90%		95%	
combination	PD7	TC7	PD7	TC7	PD7	TC7	PD7	TC7
c1	0.96	1.44	0.23	0.80	0.05	0.47	0.02	0.34
c2	1.35	3.16	0.63	2.82	0.51	2.53	0.58	2.35
c3	0.23	0.24	0.25	0.56	0.28	1.47	0.32	3.11
c4	0.62	1.14	0.86	0.83	1.28	0.79	1.71	0.85

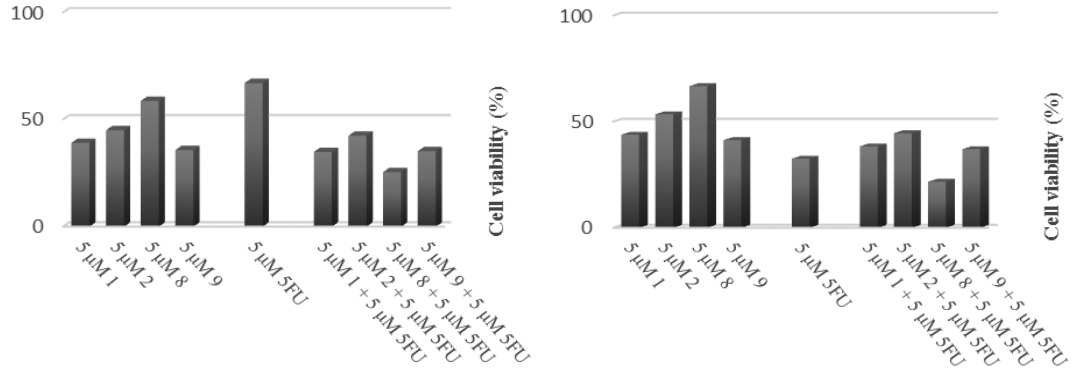

Figure 7. Cell viability of Caco-2/PD7 (A) and Caco-2/TC7 (B) after treatment with different combinations and compounds.

Table 6. DRI Values or Drugs in Different Combinations[a]

	1		2		8		9		5-FU	
	50%	75%	50%	75%	50%	75%	50%	75%	50%	75%
					Caco-2/PD7					
c1	1.13	4.97							12.74	40.62
c2			0.84	2.61					6.16	3.97
c3					5.50	4.54			19.66	35.19
c4							1.85	1.21	13.32	37.16
					Caco-2/TC7					
c1	1.72	2.36							1.16	2.66
c2			1.40	1.40					0.41	0.48
c3					19.51	4.87			5.11	2.82
c4							2.80	2.13	1.28	2.77

[a][Au(Spy)(PTA-CH_2-*p*-COOH-C_6H_4)]Br (**1**), [Au(Spyrim)(PTA-CH_2-*p*-COOH-C_6H_4)]Br (**2**), [Au(SMe_2pyrim)(PTA-CH_2-*p*-CH_2COOH-C_6H_4)]Br (**8**), and [Au(Spy)(PTA-CH_2-*p*-NO_2-C_6H_4)]Br (**9**).

The higher the DRI value, the greater the dose reduction achieved by the combination of drugs, which can lead to a decrease of the toxicity and side effects. For the combination experiments on Caco-2/PD7 cells, most of the complexes undergo a decrease of the needed dose, especially in the case of 5-FU, for which a dose 40 times lower is needed for a 75% growth inhibition effect when in combination with **1** than by itself. The DRI is not as accused for the experiments involving Caco-2/TC7 cells.

2.5. Studies on the Mechanism. *2.5.1. Apoptosis and Cell Cycle Studies.* In order to know the type of cell death triggered by our compounds, we performed some apoptosis assays with the Caco-2 cells (PD7 and TC clones) with complex **1**, which has shown the lowest IC_{50} values in both clones. Its ability to induce apoptosis was studied by flow cytometry over time, by a combination of the apoptotic markers propidium iodide (PI) and anexinV, and compared to control, nontreated cells and to the reference drugs auranofin and cisplatin (Figure S69 and Table S4). Caco-2/PD7 cells treated with complex **1** (with a dosage equal to its IC_{50} concentration) show a reduction in the proportion of living cells over time, with a concomitant increase in cells undergoing apoptosis (in early and late stages) and negligible necrotic cells, similar to treatment with the benchmark drug auranofin. However, cells treated with cisplatin remain very similar to control cells, with the exception of an increase of the proportion of necrotic cells and a decrease of living cells.

In the case of the Caco-2/TC7 clone, control cells show an inhibition of the apoptotic process because 86.4% of cells are viable, and only a small proportion are undergoing cell death. This inhibition of apoptosis produces a fast growth and proliferation of cancerous cells. The effect on those cells upon treatment with the reference drugs is, again, highly dependent on the molecule used: while it seems that treatment with cisplatin does not produce much change on the cells, no viable cells can be found after treatment with auranofin, as occurred with cells treated with **1**. The main difference between complex **1** and auranofin resides in the stage of apoptosis. Thus, both clones incubated with **1** undergo apoptosis in the early stage, while the majority of cells treated with auranofin are found in

DOI: 10.1021/acs.inorgchem.7b01370
Inorg. Chem. 2017, 56, 8562−8579

the late stage of apoptosis. Figure 8 reveals a different behavior in the treatment of both clones with the gold complex.

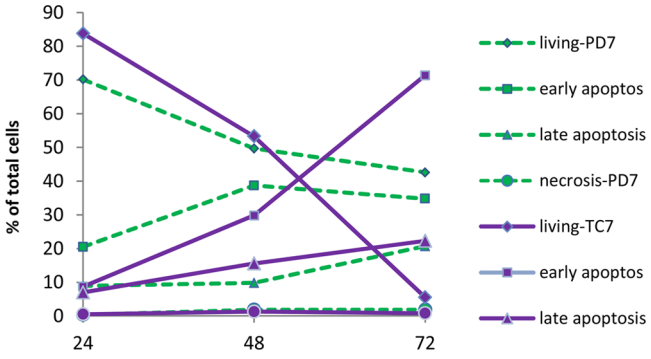

Figure 8. Representation of the data from cell death analysis on Caco-2/PD7 and Caco-2/TC7 cells after incubation with **1** over time.

Complex **1** is clearly more effective against Caco-2/TC7 cells in comparison to Caco-2/PD7 cells because there is a significant decrease in the population of living cells over time in favor of cells in early apoptosis. There is an interest in chemotherapy-induced apoptosis,[82,83] and it can be said that our thiolate complexes clearly seem to induce apoptosis in both colon cancer clones, leading to cell death in the cancerous cells.

In cancer research, it is important to study the cell cycle of cancerous cells and the possible changes induced by an anticancer drug. Here, we have studied the cell cycle of Caco-2/PD7 and Caco-2/TC7 by flow cytometry after their incubation for 24, 48, and 72 h with complex **1** and with the reference drugs. The corresponding histograms and distribution of the cells are provided in Figure S70 and Table S5, respectively. The low percentage of cells found in the G0/G1 phases for the control samples (nontreated cells) could be indicative of the high proliferation and uncontrolled growth of cancerous cells. It would be interesting if the complexes chosen for the anticancer treatment could arrest the cell cycle at phases previous to cell division, inhibiting the proliferation of cancer cells. The reference drug used for this study, auranofin, is too toxic for the cells, and not enough living cells are found for the analysis, leading to a markedly perturbed cytometry profile. Cisplatin seems to prolong the G0/G1 and S phases, avoiding the proliferation and growth of cells. Treatment with **1** does not seem to produce an important effect on the cell cycle of Caco-2/PD7 cells, while leading to an arrest of the cell cycle of Caco-2/TC7 cells in the G0/G1 phases, with a concomitant decrease of the population in the S phase. Like the results found in auranofin, complex **1** is highly toxic for the Caco-2/TC7 cells and after 72 h of incubation, and, consequently, not enough viable cells remained for cell cycle population calculation. These results are in agreement with the data obtained with similar gold(I) thiolate complexes previously described.[41,23]

2.5.2. ROS Production. Because the thioredoxin system helps to keep the redox balance inside the cells, its inhibition by gold complexes has an impact on the production of oxidative species because they can no longer be neutralized.[32] Some authors have stated that manipulation of the ROS levels may be an effective strategy for the treatment of cancer because cancerous cells are especially redox vulnerable,[84,85] and an elevated ROS production is directly related to cell death, by triggering apoptosis. On this basis, the production of hydrogen peroxide (H_2O_2) in Caco-2 cells upon treatment with the IC_{50} concentrations of some of the described gold(I) thiolates (**1**, **5**, **9**, and **13**) has been studied using the H_2O_2-sensitive fluorescent probe 2,7-dichlorodihydrofluorescein diacetate (DCFH-DA). DCFH-DA is first allowed to enter the cells, where it is hydrolyzed to 2,7-dichlorodihydrofluorescein by the action of estearases. This molecule is then oxidized by H_2O_2 present in the cell to yield a fluorescent product, namely, 2,7-dichlorofluorescein (DCF). To study whether the cell death induced by the gold thiolate derivatives is dependent on the ROS levels, Caco-2/TC7 cells were treated with complexes **1**, **5**, **9**, and **13** at their IC_{50} concentrations, and the fluorescence intensity of DCF was measured, which is an indicator of the formation of H_2O_2 over time. There is low emission within the first 60 min of the experiment, which is increased thereafter, indicating ROS formation, after gold complexes have entered the cells. As can be seen in Figure 9, the four compounds cause an increase in the DCF fluorescence signals compared with the vehicle treated cells, which is more marked in the case of complex **1**. This increase in the ROS levels has also been observed in previously reported gold(I) derivatives.[54,86]

2.5.3. Interaction with Reductase Systems. The main function of the thioredoxin system and other reductase systems like the glutathione system is to control the redox state inside the cell, contributing, for example, to the removal of H_2O_2.[87] An overexpression of thioredoxin and TrxR has been found in some cancerous cells in tumors, related to aggressive tumor growth and inhibition of apoptosis.[88] For this reason, the thioredoxin system has been considered to be an appropriate target for the development of new drugs,[88,89] in special metallic

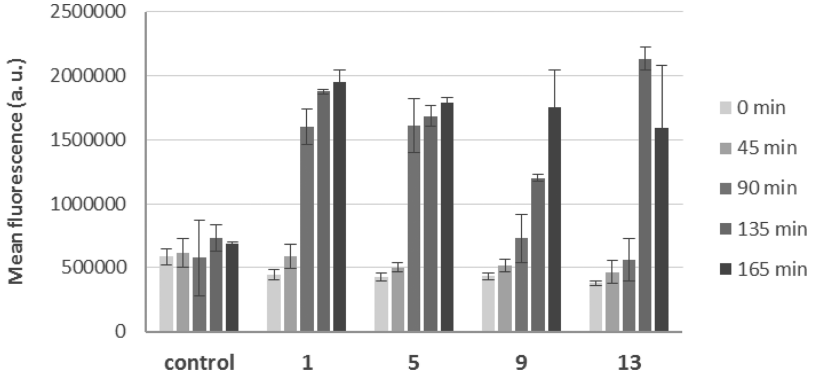

Figure 9. Quantification of the ROS by the DCFH-DA method in Caco-2/TC7 cells after treatment with compounds **1**, **5**, **9**, and **13** at their IC_{50} concentrations.

DOI: 10.1021/acs.inorgchem.7b01370
Inorg. Chem. 2017, 56, 8562−8579

complexes that can act as inhibitors of TrxR.[32,85,90−92] The key factor for interaction of the metal complexes and TrxR is the presence of cysteine and Sec residues found in the catalytic sites of the enzyme, which can bind soft metals such as platinum(II) and gold(I), with the consequent inhibition of the enzyme.[91,32,90] Inhibition of the enzyme would lead to a high production of ROS and ROS-induced apoptosis.[90,91,93]

A preliminary experiment, based on the reduction of 5,5′-dithiobis(2-nitrobenzoic) acid (DTNB) with nicotinamide adenine dinucleotide phosphate (NADPH) to 5-thio-2-nitrobenzoic acid (TNB), was performed to study inhibition of the thiol reductase activity in Caco-2/TC7 cell lysates after treatment for 24 h with **1** at its IC_{50} concentration. An increase in the activity of antioxidant enzymes that can reduce DTNB was found (see Figure 10). DTNB is not selective to TrxR:

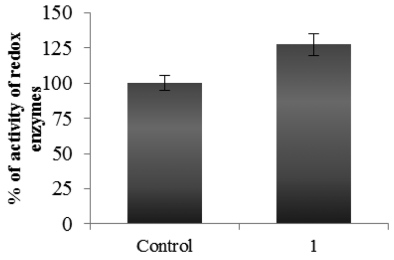

Figure 10. Thiol reductase activity in Caco-2 cell lysates after treatment with **1**.

other enzymes such as GR and GPx can also reduce DTNB. This increase could be given by a defense mechanism developed by the cells: if the compounds are interacting with TrxR, there is an increase of ROS production, and cells would increase their production of antioxidant enzymes to be able to overcome the oxidative damage produced by ROS. A similar effect was found by Illán-Cabeza et al.[94] on glioma tumors upon treatment with a phosphanegold(I) complex. They found increased production of glutathione and increased activity of antioxidant enzymes such as superoxide dismutase and GPx compared to nontreated tumor mice models and healthy mice, which is a defense mechanism of the cell to reduce the ROS formed after inhibition of TrxR.

In order to specifically study the interaction with TrxR, a preliminary study on the in vitro inhibition of human thioredoxin reductase 1 (TrxR1) was performed. Its activity was studied after incubation for 24 h with 4 μM **1**, **9**, and auranofin as positive controls at their IC_{50} concentrations (Figure 11). This activity is measured as an increase of the absorbance at 412 nm. Treatment with auranofin reduced the activity of the enzyme to 76%, while compounds **1** and **9** led to decreases of the activity to 62 and 65%, respectively. Inhibition

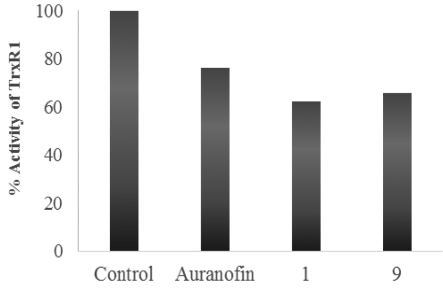

Figure 11. Inhibitory effects of auranofin, **1**, and **9** on TrxR1.

of the TrxR activity has also been previously found in related gold(I) derivatives.[26,54,95−97]

3. CONCLUSIONS

Here we report the synthesis of new gold(I) thiolate derivatives with water-soluble phosphanes derived from PTA via [{Au(thiolate}$_n$] formation with good yields. These compounds were screened for their antiproliferative effects on human colon cancer cell lines and found to be potent cytotoxic agents. All of the compounds have demonstrated more chemical stability in buffered solutions and higher anticancer activity than the previous derivatives with the same phosphanes but with halogen or pseudohalogen ligands. This fact supports the relevance of the appropriate choice of ligands in the coordination sphere of the metallic center. Thus, thiolate ligands confer higher stability under physiological conditions, which leads to an improvement of their effectiveness as cytotoxic derivatives. Besides the relevance of the thiolate incorporation, the presence of electron-withdrawing substituents ($-NO_2$) in the para position of the benzene moiety in the alkylated PTA phosphane improves the stability and lipophilicity, although without improvement of the anticancer activity. Moderate binding constant values for interaction of the compounds with BSA have been calculated, which makes them suitable for transportation by the protein through blood and easy release to the target. Some of these new compounds have demonstrated a selective cytotoxic behavior because high viabilities (values around 100%) have been found in normal enterocytes (Caco-2 cells under confluence) and synergism with 5-FU when is administered in combination with gold derivatives to cancerous cells, leading to a reduction of up to 40 times the dose required of 5-FU for the same effect. Preliminary studies of the possible mechanism allowed us to conclude that the complexes described here induce apoptosis and an increase in the intracellular ROS levels, probably due to interaction with the enzyme TrxR altering, as a consequence, the redox balance.

4. EXPERIMENTAL SECTION

4.1. General Procedures. All of the reactions were carried out under an argon atmosphere using common Schlenk techniques. Proton (^{1}H), phosphorus (^{31}P), and carbon (^{13}C) (100.62 MHz) NMR spectra were recorded on a Bruker Avance 400 spectrometer (400 MHz for ^{1}H; 161.97 MHz for ^{31}P; 100.62 MHz for ^{13}C) using DMSO-d_6 as the solvent. The peak positions are relative to external tetramethylsilane (^{1}H and ^{13}C) or 85% hydrogen phosphate (^{31}P) and given in parts per million (ppm). Coupling constants are reported in hertz. MALDI mass spectrometry (MS) spectra were measured on a Micromass Autospec spectrometer in positive-ion mode using dithranol or *trans*-2-[3-(4-*tert*-butylphenyl)-2-methyl-2-propenylidene]malononitrile as the matrix. IR spectra were recorded on a PerkinElmer Spectrum One Fourier transform infrared spectrometer. The samples were measured in the solid state using an ATR accessory that covers a wavelength range from 4000 to 200 cm^{-1}. UV−vis absorption spectra were recorded on a Thermo Scientific Evolution 600 spectrophotometer from solutions in quartz cuvettes (1 cm optical path). Elemental analyses were obtained in house using a PerkinElmer 2400 series II CHNS/O system analyzer. Fluorescence emission spectra were recorded on a Jobin-Yvon-Horiba Fluorolog FL-3-11 spectrophotometer using quartz cuvettes (1 cm optical path) for samples in solution.

4.2. Materials. The phosphanes PTA, [PTA-CH_2-*p*-COOH-C_6H_4]Br, [PTA-CH_2-*p*-CH_2COOH-C_6H_4]Br, [PTA-CH_2-*p*-NO_2-C_6H_4]Br, and [PTA-CH_2-CONH-CH(CH_2Ph)COOMe]Br were synthesized as described elsewhere.[44] The gold reagent [AuCl(tht)]

DOI: 10.1021/acs.inorgchem.7b01370
Inorg. Chem. 2017, 56, 8562−8579

was prepared as described by Uson et al.[98] All chemicals were of reagent grade and were used as received by commercial suppliers.

4.3. General Procedure for the Synthesis of Complexes 1–13. The reactions were carried out on a one-pot basis. NaOEt (0.22 mmol, 14.97 mg) was added to an ethanolic solution of the corresponding HSR [0.2 mmol; Spy, 22.23 mg; Spyrim, 22.43 mg; S(Me)pyrim, 32.50 mg; S(Me)$_2$pyrim, 28.04 mg]. The mixture was allowed to react for 15 min, and [AuCl(tht)] (0.2 mmol, 64.12 mg) was added next to the solution. The suspension formed was stirred for 2 h, and then the solid and solution were separated by removing the liquid phase. The corresponding phosphane (0.19 mmol) was then added to the suspension with 20 mL of acetone. The resulting suspension was stirred overnight. After this time, the solid was filtered, washed with cold acetone and diethyl ether, and allowed to dry.

*4.3.1. [Au(Spyridine)(PTA-CH$_2$-p-COOH-C$_6$H$_4$) (**1**).* Yield: light-green solid, 81%. ^{1}H NMR (400 MHz, DMSO-d_6, 25 °C): δ 8.07 and 7.69 (AA′XX′ system, 4H, H_{Ph}), 7.99 (d, J = 6.9 Hz, 1H, H_{Py}), 7.39 (t, J = 6.9 Hz, 1H, H_{Py}), 7.33 (d, J = 6.9 Hz, 1H, H_{Py}), 6.85 (t, J = 6.9 Hz, 1H, H_{Py}), 5.19 and 4.99 (AB system, J_{AB} = 8.0 Hz, 4H, N$^+$CH_2N), 4.65 (br s, 2H, N$^+$CH_2P), 4.58 and 4.32 (AB system, J_{AB} = 20 Hz, NCH_2N), 4.31 (s, 2H, N$^+$CH_2Ph), 4.31–4.16 (m, 4H, NCH_2P). ^{31}P{^{1}H} NMR (162 MHz, DMSO-d_6, 25 °C): δ −35.6. ^{13}C{^{1}H} NMR (101 MHz, DMSO-d_6, 25 °C): δ 166.9 (s, 1C, COOH), 136.1 (s, 2C, C_{Py}), 133.4 (s, 2C, C_{Ph}), 132.6 (s, 1C, C_{Ph}), 130.0 (s, 1C, C_{Py}), 129.9 (s, 1C, C_{Ph}), 129.8 (s, 2C, C_{Ph}), 129.5 (s, 1C, C_{Py}), 116.4 (s, 1C, C_{Py}), 78.9 (d, J = 3.1 Hz, 2C, N$^+$CH$_2$N), 68.8 (d, J = 7.1 Hz, 1C, NCH$_2$N), 64.0 (s, 1C, N$^+$CH$_2$Ph), 52.2 (br s, 1C, N$^+$CH$_2$P), 47.1 (d, J = 12.2 Hz, 2C, NCH$_2$P). IR: ν_{max} 1690 (CO), 552 (Au–S) cm^{-1}. MALDI MS: m/z 599 (1%, [M]$^+$), 419 (100%, [Au(Spy)$_2$ + H]$^+$), 307 (41%, [Au(Spy)]). Elem anal. Calcd for $C_{19}H_{23}AuBrN_4O_2PS$ (679.32): C, 33.59; H, 3.41; N, 8.25; S, 4.72. Found: C, 33.26; H, 4.00; N, 8.13; S, 5.36. $S_{25\ °C}(H_2O)$ = 1.84 g L^{-1}.

*4.3.2. [Au(Spyrimidine)(PTA-CH$_2$-p-COOH-C$_6$H$_4$)]Br (**2**).* Yield: yellowish-green solid, 87%. ^{1}H NMR (400 MHz, DMSO-d_6, 25 °C): δ 10.01 (s, 1H, COOH), 8.31 (d, J = 4.8 Hz, 2H, H_{Pyrim}), 8.07 and 7.68 (AA′XX′ system, 4H, H_{Ph}), 6.94 (t, J = 4.8 Hz, 1H, H_{Pyrim}), 5.24 and 5.02 (AB system, J_{AB} = 8.0 Hz, 4H, N$^+$CH_2N), 4.68 (br s, 2H, N$^+$CH_2P), 4.63–4.15 (m, 6H, NCH_2N, NCH_2P). ^{31}P{^{1}H} NMR (162 MHz, DMSO-d_6, 25 °C): δ −38.4. ^{13}C{^{1}H} NMR (101 MHz, DMSO-d_6, 25 °C): δ 166.8 (s, 1C, COOH), 155.8 (s, 2C, C_{Pyrim}), 133.4 (s, 2C, C_{Ph}), 132.5 (s, 1C, C_{Ph}), 130.0 (s, 1C, C_{Ph}), 129.8 (s, 2C, C_{Ph}), 78.8 (s, 2C, N$^+$CH$_2$N), 68.8 (s, 1C, NCH$_2$N), 63.8 (s, 1C, N$^+$CH$_2$Ph), 52.1 (br s, 1C, N$^+$CH$_2$P), 47.0 (d, J = 9.9 Hz, 2C, NCH$_2$P). IR: ν_{max} 1687 (CO), 552 (Au–S) cm^{-1}. MALDI MS: m/z 600.08 (2%, [M]$^+$), 308.98 (59%, [Au(Spyrim)]$^+$), 354.03 (21%, [Au(PTA)]$^+$), 511.08 (11%, [Au(PTA)$_2$]$^+$). Anal. Calcd for $C_{18}H_{22}AuBrN_5O_2PS$ (680.31): C, 31.78; H, 3.26; N, 10.29; S, 4.71. Found: C, 31.36; H, 3.72; N, 10.16; S, 4.52. $S_{25\ °C}(H_2O)$ = 3.58 g L^{-1}.

*4.3.3. [Au(S(Me)pyrimidine)(PTA-CH$_2$-p-COOH-C$_6$H$_4$)]Br (**3**).* Yield: light-yellow solid, 85%. ^{1}H NMR (400 MHz, DMSO-d_6, 25 °C): δ 10.11 (s, 1H, COOH), 8.17 (d, J = 5.1 Hz, 1H, H_{Pyrim}), 8.07 and 7.69 (AA′XX′ system, 4H, H_{Ph}), 6.86 (d, J = 5.1 Hz, 1H, H_{Pyrim}), 5.28 and 5.05 (AB system, J_{AB} = 12.0 Hz, 4H, N$^+$CH_2N), 4.69 (br s, 2H, N$^+$CH_2P), 4.60 and 4.37 (AB system, J_{AB} = 16.0 Hz, 2H, NCH_2N), 4.40 (s, 2H, N$^+$CH_2Ph), 4.38–4.19 (m, 4H, NCH_2P), 2.26 (s, 3H, CH_3). ^{31}P{^{1}H} NMR (162 MHz, DMSO-d_6, 25 °C): δ −32.4. ^{13}C{^{1}H} NMR (101 Hz, DMSO-d_6, 25 °C): δ 166.8 (s, 1C, COOH), 156.9 (s, 1C, C_{Pyrim}), 136.4 (s, 2C, C_{Ph}), 132.5 (s, 1C, C_{Ph}), 129.9 (s, 1C, C_{Ph}), 129.8 (s, 2C, C_{Ph}), 129.5 (s, 1C, C_{Pyrim}), 116.3 (s, 2C, C_{Pyrim}), 78.7 (s, 2C, N$^+$CH$_2$N), 68.7 (s, 1C, NCH$_2$N), 63.7 (s, 1C, N$^+$CH$_2$Ph), 52.0 (d, J = 13.2 Hz, 1C, N$^+$CH$_2$P), 47.3 (d, J = 15.7 Hz, 2C, NCH$_2$P), 23.5 (s, 1C, SMePyrim). IR: ν_{max} 1688 (CO), 553 (Au–S) cm^{-1}. MALDI MS: m/z 323.00 (100%, [Au(Spyrim) + H]$^+$), 567.94 (36%, [M − Spyrim − H + Br]). Anal. Calcd for $C_{19}H_{24}AuBrN_5O_2PS{\cdot}3H_2O$ (748.38): C, 30.49; H, 4.04; N, 9.36; S, 4.28. Found: C, 30.43; H, 3.86; N, 9.21; S, 4.01. $S_{25\ °C}(H_2O)$ < 0.5 g L^{-1}.

*4.3.4. [Au(S(Me)$_2$Pyrimidine)(PTA-CH$_2$-p-COOH-C$_6$H$_4$)]Br (**4**).* Yield: light-yellow solid, 74%. ^{1}H NMR (400 MHz, DMSO-d_6, 25 °C): δ 8.05 and 7.66 (AA′XX′ system, 4H, H_{Ph}), 6.75 (s, 1H, H_{Pyrim}), 5.19 and 5.03 (AB system, J_{AB} = 12.0 Hz, 4H, N$^+$CH_2N), 4.64 (br s, 2H, N$^+$CH_2P), 4.44 (s, 2H, N$^+$CH_2Ph), 4.60 and 4.34 (AB system, J_{AB} = 12.0 Hz, 2H, NCH_2N), 4.42–4.22 (m, 4H, NCH_2P), 2.20 (s, 6H, CH_3). ^{31}P{^{1}H} NMR (162 MHz, DMSO-d_6, 25 °C): δ −26.1. ^{13}C{^{1}H} NMR (101 MHz, DMSO-d_6, 25 °C): δ 167.2 (s, 1C, COOH), 148.8 (s, 1C, C_{Pyrim}), 139.5 (s, 1C, C_{Ph}), 134.7 (s, 2C, C_{Ph}), 132.5 (s, 1C, C_{Ph}), 123.9 (s, 2C, C_{Ph}), 124.7 (s, 1C, C_{Ph}), 114.62 (s, 1C, C_{Pyrim}), 79.1 (br s, 2C, N$^+$CH$_2$N), 68.7 (br s, 1C, NCH$_2$N), 63.1 (s, 1C, N$^+$CH$_2$Ph), 52.2 (br s, 1C, N$^+$CH$_2$P), 47.5 (d, J = 22.3 Hz, 2C, NCH$_2$P), 23.4 (s, 2C, CH$_3$). IR: ν_{max} 1699 (CO), 548 (Au–S) cm^{-1}. MALDI MS: m/z 628.14 (9%, [M]$^+$), 494.13 (100%, [Au(Spyrim)-(PTA) + H]). Anal. Calcd for $C_{20}H_{26}AuBrN_5O_2PS$ (708.36): C, 33.91; H, 3.69; N, 9.89; S, 4.53. Found: C, 33.56; H, 3.95; N, 9.40; S, 4.95. $S_{25\ °C}(H_2O)$ = 2.49 g L^{-1}.

*4.3.5. [Au(Spyridine)(PTA-CH$_2$-p-CH$_2$COOH-C$_6$H$_4$)]Br (**5**).* Yield: light-green solid, 70%. ^{1}H NMR (400 MHz, DMSO-d_6, 25 °C): δ 8.11 (d, J = 3.9 Hz, 1H, H_{Py}), 7.49 and 7.44 (AA′XX′ system, 4H, H_{Ph}), 7.37 (td, J = 8.0 and 1.8 Hz, 1H, H_{Py}), 7.32–7.21 (m, 1H, H_{Py}), 6.90 (t, J = 6.0 Hz, 1H, H_{Py}), 5.17 and 4.97 (AB system, J_{AB} = 12.0 Hz, 4H, N$^+$CH_2N), 4.62 (br s, 2H, N$^+$CH_2P), 4.59 and 4.33 (AB system, J_{AB} = 12.0 Hz, NCH_2N), 4.36–4.25 (m, 4H, NCH_2P), 4.24 (s, 2H, N$^+$CH_2Ph), 3.66 (s, 2H, HOOC-CH_2-Ph). ^{31}P{^{1}H} NMR (162 MHz, DMSO-d_6, 25 °C): δ −28.8. ^{13}C{^{1}H} NMR (101 Hz, DMSO-d_6, 25 °C): δ 175.2 (s, 1C, COOH), 148.4 (s, 1C, C_{Py}), 137.5 (s, 1C, C_{Ph}), 135.6 (s, 1C, C_{Py}), 132.9 (s, 2C, C_{Ph}), 130.2 (s, 2C, C_{Ph}), 126.1 (s, 1C, C_{Py}), 123.5 (s, 1C, C_{Ph}), 121.8 (s, 1C, C_{Py}), 118.2 (s, 1C, C_{Py}), 78.7 (d, J = 4.3 Hz, 2C, N$^+$CH$_2$N), 68.8 (d, J = 5.5 Hz, 1C, NCH$_2$N), 64.3 (s, 1C, N$^+$CH$_2$Ph), 52.0 (d, J = 15.4 Hz, 1C, N$^+$CH$_2$P), 47.3 (d, J = 16.8 Hz, 2C, NCH$_2$P), 40.0 (s, 1C, HOOC-CH$_2$-Ph). IR: ν_{max} 1697 (CO), 550 (S–Au) cm^{-1}. MALDI MS: m/z 613.14 (32%, [M]$^+$), 502.15 (14%, [M − Spy − H]$^+$). Anal. Calcd for $C_{20}H_{25}AuBrN_4O_2PS$ (693.35): C, 34.65; H, 3.63; N, 8.08; S, 4.62. Found: C, 34.35; H, 3.85; N, 8.32; S, 4.27. $S_{25\ °C}(H_2O)$ < 0.5 g L^{-1}.

*4.3.6. [Au(Spyrimidine)(PTA-CH$_2$-p-CH$_2$COOH-C$_6$H$_4$)]Br (**6**).* Yield: light-green powder, 89%. ^{1}H NMR (400 MHz, DMSO-d_6, 25 °C): δ 9.97 (s, 1H, COOH), 8.31 (d, J = 4.8 Hz, 2H, H_{Pyrim}), 7.48 and 7.43 (AA′XX′ system, 4H, H_{Ph}), 6.96 (t, J = 4.8 Hz, 1H, H_{Pyrim}), 5.12 and 4.97 (AB system, J_{AB} = 8.0 Hz, 4H, N$^+$CH_2N), 4.56 (br s, 2H, N$^+$CH_2P), 4.57 and 4.34 (AB system, J_{AB} = 16.0 Hz, 2H, NCH_2N), 4.30 (s, 2H, N$^+$CH_2Ph), 4.28–4.15 (m, 4H, NCH_2P), 3.69 (s, 2H, HOOC-CH_2-Ph). ^{31}P{^{1}H} NMR (162 MHz, DMSO-d_6, 25 °C): δ −37.3. ^{13}C{^{1}H} NMR (101 Hz, MeOD, 25 °C): δ 175.0 (s, 1C, COOH), 157.9 (s, 2C, C_{Pyrim}), 139.5 (s, 1C, C_{Ph}), 134.2 (s, 2C, C_{Ph}), 131.7 (s, 2C, C_{Ph}), 124.7 (s, 1C, C_{Ph}), 116.7 (s, 1C, C_{Pyrim}), 80.9 (d, J = 4.2 Hz, 2C, N$^+$CH$_2$N), 70.8 (d, J = 6.1 Hz, 1C, NCH$_2$N), 66.7 (s, 1C, N$^+$CH$_2$Ph), 55.0 (d, J = 9.4 Hz, 1C, N$^+$CH$_2$P), 49.9 (br s, 2C, NCH$_2$P), 41.6 (s, 1C, HOOC-CH$_2$-Ph). IR: ν_{max} 1696 (CO), 552 (S–Au) cm^{-1}. MALDI MS: m/z 614.13 (12%, [M]$^+$), 502.13 (24%, [M − Spyrim − H]). Anal. Calcd for $C_{19}H_{24}AuBrN_5O_2PS$ (694.34): C, 32.87; H, 3.48; N, 10.09; S, 4.62. Found: C, 32.34; H, 4.01; N, 9.68; S, 4.40. $S_{25\ °C}(H_2O)$ = 3.60 g L^{-1}.

*4.3.7. [Au(S(Me)Pyrimidine)(PTA-CH$_2$-p-CH$_2$COOH-C$_6$H$_4$)]Br (**7**).* Yield: yellow solid, 53%. ^{1}H NMR (400 MHz, DMSO-d_6, 25 °C): δ 9.97 (s, 1H, COOH), 8.16 (d, J = 5.1 Hz, 2H, H_{Pyrim}), 7.48 and 7.42 (AA′XX′ system, 4H, H_{Ph}), 6.87 (d, J = 5.1 Hz, 1H, H_{Pyrim}), 5.13 and 4.97 (AB system, J_{AB} = 8.0 Hz, 4H, N$^+$CH_2N), 4.59 (br s, 2H, N$^+$CH_2P), 4.56–4.20 (m, 8H, NCH_2N, N$^+$CH_2Ph, NCH_2P), 3.69 (s, 2H, HOOC-CH_2-Ph), 2.25 (s, 3H, CH_3-Spyrim). ^{31}P{^{1}H} NMR (162 MHz, DMSO-d_6, 25 °C): δ −30.6. ^{13}C{^{1}H} NMR (101 Hz, MeOD, 25 °C): δ 175.1 (s, 1C, COOH), 156.9 (s, 2C, C_{Pyrim}), 139.7 (s, 1C, C_{Ph}), 134.2 (s, 2C, C_{Ph}), 131.7 (s, 2C, C_{Ph}), 124.4 (s, 1C, C_{Ph}), 116.3 (s, 2C, C_{Pyrim}), 80.9 (s, 2C, N$^+$CH$_2$N), 70.5 (s, 1C, NCH$_2$N), 66.6 (s, 1C, N$^+$CH$_2$Ph), 54.4 (br s, 1C, N$^+$CH$_2$P), 49.2 (br s, 2C, NCH$_2$P), 41.7 (s, 1C, HOOC-CH$_2$-Ph), 24.0 (s, 1C, SMePyrim). IR: ν_{max} 1694 (CO), 557 (S–Au) cm^{-1}. MALDI MS: m/z 628.23 (75%, [M]$^+$), 502.19 (90%, [M − Spyrim − H]$^+$), 582.11 (12%, [M − Spyrim + Br]$^+$). Anal. Calcd for $C_{20}H_{26}AuBrN_5O_2PS$ (708.36): C, 33.91; H, 3.70; N, 9.9; S, 4.53. Found: C, 34.45; H, 4.11; N, 9.57; S, 3.14. $S_{25\ °C}(H_2O)$ = 0.49 g L^{-1}.

*4.3.8. [Au(S(Me)$_2$Pyrimidine)(PTA-CH$_2$-p-CH$_2$COOH-C$_6$H$_4$)]Br (**8**).* Yield: greenish yellow solid, 65%. ^{1}H NMR (400 MHz, DMSO-d_6, 25

DOI: 10.1021/acs.inorgchem.7b01370
Inorg. Chem. 2017, 56, 8562–8579

°C): δ 9.99 (s, 1C, COOH), 7.50 and 7.44 (AA′XX′ system, 4H, H_{Ph}), 6.75 (s, 1H, H_{Pyrim}), 5.25 and 5.03 (AB system, J_{AB} = 12.0 Hz, 4H, N^+CH_2N), 4.68 (d, J = 4.3 Hz, 2H, N^+CH_2P), 4.60 and 4.35 (AB system, J_{AB} = 16.0 Hz, 2H, NCH_2N), 4.40−4.26 (m, 6H, N^+CH_2Ph, NCH_2P), 3.66 (s, 2H, HOOC-CH_2-Ph), 2.21 (s, 6H, CH_3). $^{31}P\{^1H\}$ NMR (162 MHz, DMSO-d_6, 25 °C): δ −26.4. $^{13}C\{^1H\}$ NMR (101 Hz, DMSO-d_6, 25 °C): δ 172.2 (s, 1C, COOH), 165.3 (s, 2C, C_{Pyrim}), 137.4 (s, 1C, C_{Ph}), 132.9 (s, 2C, C_{Ph}), 130.1 (s, 2C, C_{Ph}), 123.6 (s, 1C, C_{Ph}), 114.6 (s, 1C, C_{Pyrim}), 78.6 (d, J = 4.4 Hz, 2C, N^+CH_2N), 68.7 (d, J = 6.2 Hz, 1C, NCH_2N), 64.1 (s, 1C, N^+CH_2Ph), 51.8 (d, J = 19.2 Hz, 1C, N^+CH_2P), 47.4 (d, J = 20.0 Hz, 2C, NCH_2P), 40.0 (s, 1C, HOOC-CH_2-Ph), 23.4 (s, 2C, CH_3). IR: ν_{max} 1702 (CO), 549 (S−Au) cm^{-1}. MALDI MS: m/z 642.01 (16%, $[M]^+$), 502.01 (8%, [M − Spyrim − $H]^+$), 476.96 (25%, $[Au(Spyrim)_2 + H]^+$). Anal. Calcd for $C_{21}H_{28}AuBrN_5O_2PS$ (722.39): C, 34.92; H, 3.91; N, 9.69; S, 4.44. Found: C, 34.88; H, 4.08; N, 9.33; S, 4.91. $S_{25\ °C}(H_2O)$ < 0.5 g L^{-1}.

4.3.9. [Au(Spyridine)(PTA-CH_2-p-C_6H_4-NO_2)]Br (9). Yield: yellow solid, 47%. ^1H NMR (400 MHz, DMSO-d_6, 25 °C): δ 8.38 and 7.86 (AA′XX′ system, 4H, H_{Ph}), 7.94 (d, J = 4.4 Hz, 1H, H_{Py}), 7.41 (m, 1H, H_{Py}), 7.31 (d, J = 8.3 Hz, 1H, H_{Py}), 6.85 (ddd, J = 6.9, 5.6, and 1.1 Hz, 1H, H_{Py}), 5.23 and 5.02 (AB system, J_{AB} = 12.0 Hz, 4H, N^+CH_2N), 4.64 (br s, 2H, N^+CH_2P), 4.59 and 4.35 (AB system, J_{AB} = 16.0 Hz, 2H, NCH_2N), 4.43 (s, 2H, N^+CH_2Ph), 4.34−4.14 (m, 4H, NCH_2P). $^{31}P\{^1H\}$ NMR (162 MHz, DMSO-d_6, 25 °C): δ −37.5. $^{13}C\{^1H\}$ NMR (101 Hz, DMSO-d_6, 25 °C): δ 148.8 (s, 1C, C_{Ph}), 136.6 (s, 1C, C_{Py}), 134.7 (s, 2C, C_{Ph}), 132.7 (s, 1C, C_{Ph}), 129.3 (s, 1C, C_{Py}), 123.9 (s, 2C, C_{Ph}), 116.2 (s, 1C, C_{Py}), 79.0 (d, J = 4.5 Hz, 2C, N^+CH_2N), 68.8 (d, J = 7.0 Hz, 1C, NCH_2N), 63.1 (s, 1C, N^+CH_2Ph), 52.2 (d, J = 9.4 Hz, 1C, N^+CH_2P), 47.1 (d, J = 12.6 Hz, 2C, NCH_2P). IR: ν_{max} 1519, 1347, and 851 (NO_2) cm^{-1}. MALDI MS: m/z 600.05 (23%, $[M]^+$), 418.98 (45%, $[Au(Spy)_2 + H]$). Anal. Calcd for $C_{18}H_{22}AuBrN_5O_2PS$ (680.31): C, 31.78; H, 3.26; N, 10.29; S, 4.71. Found: C, 32.01; H, 3.87; N, 10.29; S, 4.74. $S_{25\ °C}(H_2O)$ < 0.5 g L^{-1}.

4.3.10. [Au(Spyrimidine)(PTA-CH_2-p-C_6H_4-NO_2)]Br (10). Yield: light-green solid, 70%. ^1H NMR (400 MHz, DMSO-d_6, 25 °C): δ 8.38 and 7.87 (AA′XX′ system, 4H, H_{Ph}), 8.32 (d, J = 4.9 Hz, 2H, H_{Pyrim}), 6.94 (t, J = 4.9 Hz, 1H, H_{Pyrim}), 5.29 and 5.06 (AB system, J_{AB} = 8.0 Hz, 4H, N^+CH_2N), 4.71 (br s, 2H, N^+CH_2P), 4.59 and 4.35 (AB system, J_{AB} = 16.0 Hz, 2H, NCH_2N), 4.43 (s, 2H, N^+CH_2Ph), 4.34−4.14 (m, 4H, NCH_2P). $^{31}P\{^1H\}$ NMR (162 MHz, DMSO-d_6, 25 °C): δ −31.4. $^{13}C\{^1H\}$ NMR (101 Hz, DMSO-d_6, 25 °C): δ 159.8 (s, 2C, C_{Pyrim}), 148.8 (s, 1C, C_{Ph}), 134.7 (s, 2C, C_{Ph}), 123.9 (s, 1C, C_{Pyrim}), 113.3 (s, 1C, C_{Pyrim}), 78.9 (s, 2C, N^+CH_2N), 68.7 (d, J = 6.1 Hz, 1C, NCH_2N), 62.9 (s, 1C, N^+CH_2Ph), 52.2 (d, J = 15.9 Hz, 1C, N^+CH_2P), 47.4 (d, J = 17.3 Hz, 2C, NCH_2P). IR: ν_{max} 1518, 1350, and 851 (NO_2); 549 (Au−S) cm^{-1}. MALDI MS: m/z 601.05 (12%, $[M]^+$), 354.1 (15%, $[Au(PTA)]^+$), 420.98 (5%, $[Au(Spyrim)_2 + H]$), 489.0 (21%, [M − Spyrim − H]), 568.9 (10%, [M − Spyrim + $Br]^+$). Anal. Calcd for $C_{17}H_{21}AuBrN_6O_2PS$ (681.30): C, 29.97; H, 3.11; N, 12.34; S, 4.71. Found: C, 30.15; H, 3.19; N, 12.58; S, 4.86. $S_{25\ °C}(H_2O)$ = 2.54 g L^{-1}.

4.3.11. [Au(S(Me)Pyrimidine)(PTA-CH_2-p-C_6H_4-NO_2)]Br (11). Yield: light-green solid, 83%. ^1H NMR (400 MHz, DMSO-d_6, 25 °C): δ 8.37 and 7.88 (AA′XX′ system, 4H, H_{Ph}), 8.17 (d, J = 5.1 Hz, 1H, H_{Pyrim}), 6.86 (d, J = 5.1 Hz, 1H, H_{Pyrim}), 5.34 and 5.09 (AB system, J_{AB} = 12.0 Hz, 4H, N^+CH_2N), 4.77 (d, J = 3.6 Hz, 2H, N^+CH_2P), 4.59 and 4.37 (AB system, J_{AB} = 12.0 Hz, 2H, NCH_2N), 4.52 (s, 2H, N^+CH_2Ph), 4.43−4.24 (m, 4H, NCH_2P), 2.26 (s, 3H, CH_3). $^{31}P\{^1H\}$ NMR (162 MHz, DMSO-d_6, 25 °C): δ −26.1. $^{13}C\{^1H\}$ NMR (101 Hz, DMSO-d_6, 25 °C): δ 178.7 (s, 1C, C_{Pyrim}), 166.4 (s, 1C, C_{Pyrim}), 155.9 (s, 1C, C_{Pyrim}), 148.8 (s, 1C, C_{Ph}), 134.7 (s, 2C, C_{Ph}), 132.6 (s, 1C, C_{Ph}), 123.9 (s, 2C, C_{Ph}), 115.2 (s, 1C, C_{Pyrim}), 78.9 (d, J = 4.9 Hz, 2C, N^+CH_2N), 68.6 (d, J = 7.2 Hz, 1C, NCH_2N), 62.8 (s, 1C, N^+CH_2Ph), 52.1 (d, J = 19.8 Hz, 1C, N^+CH_2P), 47.5 (d, J = 20.3 Hz, 2C, NCH_2P). IR: ν_{max} 1517, 1351, and 853 (NO_2); 549 (Au−S) cm^{-1}. MALDI MS: m/z 615.09 (4%, $[M]^+$), 323.00 (100%, $[Au(Spyrim) + H]^+$), 489.08 (6%, [M − Spyrim − $H]^+$). Anal. Calcd for $C_{18}H_{23}AuBrN_6O_2PS$ (695.32): C, 31.09; H, 3.33; N, 12.09; S, 4.61. Found: C, 30.71; H, 3.65; N, 11.74; S, 4.64. $S_{25\ °C}(H_2O)$ < 0.5 g L^{-1}.

4.3.12. [Au(S(Me)$_2$Pyrimidine)(PTA-CH_2-p-C_6H_4-NO_2)]Br (12). Yield: light-green solid, 45%. ^1H NMR (400 MHz, DMSO-d_6, 25 °C): δ 8.35 and 7.83 (AA′XX′ system, 4H, H_{Ph}), 6.72 (s, 1H, H_{Pyrim}), 5.20 and 5.05 (AB system, J_{AB} = 8.0 Hz, 4H, N^+CH_2N), 4.70 (br s, 2H, N^+CH_2P), 4.60 and 4.35 (AB system, J_{AB} = 12.0 Hz, 2H, NCH_2N), 4.41 (s, 2H, N^+CH_2Ph), 4.41−4.23 (m, 4H, NCH_2P), 2.21 (s, 6H, CH_3). $^{31}P\{^1H\}$ NMR (162 MHz, DMSO-d_6, 25 °C): δ −27.1. $^{13}C\{^1H\}$ NMR (101 Hz, DMSO-d_6, 25 °C): δ 166.8 (s, 2C, C_{Pyrim}), 133.4 (s, 2C, C_{Ph}), 132.6 (s, 1C, C_{Ph}), 129.8 (s, 2C, C_{Ph}), 114.2 (s, 1C, C_{Pyrim}), 78.9 (s, 2C, N^+CH_2N), 70.8 (s, 1C, NCH_2N), 68.7 (s, 1C, NCH_2N), 63.8 (s, 1C, N^+CH_2Ph), 52.0 (d, J = 18.5 Hz, 1C, N^+CH_2P), 47.4 (d, J = 19.8 Hz, 2C, NCH_2P), 23.3 (s, 1C, S*Me*Pyrim). IR: ν_{max} 1609, 1524, and 1349 (NO_2), 544 (S−Au) cm^{-1}. MALDI MS: m/z 629.12 (3%, $[M]^+$), 477.08 (100%, $[Au(Spyrim)_2 + 2H]^+$), 494.11 (49%, $[Au(Spyrim)(PTA) + H]^+$). Anal. Calcd for $C_{19}H_{25}AuBrN_6O_2PS$ (709.35): C, 32.17; H, 3.55; N, 11.85; S, 4.52. Found: C, 32.15; H, 3.12; N, 11.65; S, 4.38. $S_{25\ °C}(H_2O)$ < 0.5 g L^{-1}.

4.3.13. [Au(Spy)(PTA-CH_2-CONH-CH(CH_2Ph)COOMe)]Br (13). Yield: light-green solid, 68%. ^1H NMR (400 MHz, DMSO-d_6, 25 C): δ 9.32 (d, J = 7.6 Hz, 1H, NH), 7.91 (d, J = 4.7 Hz, 1H, H_{Py}), 7.42 (ddd, J = 8.8, 7.1, and 1.8 Hz, 1H, H_{Py}), 7.38−7.16 (m, 6H, H_{Ph} + H_{Py}), 6.85 (ddd, J = 7.3, 5.6, and 1.1 Hz, 1H, H_{Py}), 5.29 (d, J = 11.3 Hz, 1H, N^+CH_2N), 5.19 (d, J = 11.5 Hz, 1H, N^+CH_2N), 5.01 (t, J = 9.2 Hz, 2H, N^+CH_2N), 4.73−4.63 (m, 1H, $C_{\beta,Ph}H$), 4.57 (br s, 2H, N^+CH_2P), 4.54 and 4.34 (AB system, J_{AB} = 16.0 Hz, 2H, NCH_2N), 4.32−4.24 (m, 4H, NCH_2P), 3.87 and 3.73 (AB system, J_{AB} = 16.0 Hz, 2H, N^+CH_2CO), 3.67 (s, 3H, CO_2CH_3), 3.14 (dd, J = 13.7 and 5.0 Hz, 1H, $C_{\alpha,Ph}H$), 2.94 (dd, J = 13.7 and 9.6 Hz, 1H, $C_{\alpha,Ph}H$). $^{31}P\{^1H\}$ NMR (162 MHz, DMSO-d_6, 25 °C): δ −37.6. $^{13}C\{^1H\}$ NMR (101 MHz, DMSO-d_6, 25 °C): δ 171.1 (s, 1C, CO_2CH_3), 162.1 (s, 1C, CONH), 136.8 (s, 1C, C_{Py}), 136.6 (s, 1C, $C_{q,Ph}$), 129.1 (s, 2C, $C_{Ph,Ar}$), 129.0 (s, 1C, C_{Py}), 128.4 (s, 2C, $C_{Ph,Ar}$), 128.2 (s, 1C, C_{Py}), 126.9 (s, 1C, $C_{Ph,Ar}$), 80.3 (s, 2C, N^+CH_2N), 68.8 (s, 1C, NCH_2N), 60.3 (s, 1C, N^+CH_2CO), 53.5 (s, 1C, $C_{\beta,Ph}$), 53.4 (s, 1C, N^+CH_2P), 52.3 (s, 1C, CO_2CH_3), 47.2 (d, J = 13.3 Hz, 2C, NCH_2P), 36.6 (s, 1C, $C_{\alpha,Ph}$). IR: ν_{max} 3202 (N−H), 1738 (MeOO═C−), 1675 (−HNC═O) cm^{-1}. MALDI MS: m/z 377.10 (100%, [M − Au − $Spy]^+$), 684.1 (3%, $[M]^+$), 573.1 (27%, [M − Spy − $H]^+$). Anal. Calcd for $C_{23}H_{30}AuBrN_5O_2PS$ (764.42): C, 36.14; H, 3.96; N, 9.16; S, 4.19. Found: C, 32.15; H, 3.12; N, 11.65; S, 4.38.

4.4. Distribution Coefficient (log $D_{7.4}$). The *n*-octanol/water coefficients of the complexes were determined as previously reported[99] using a shake-flask method.[23] Buffered-saline distilled water (100 mL, phosphate buffer [PO_4^{3-}] = 10 mM, [NaCl] = 0.15 M, pH 7.4) and *n*-octanol (100 mL) were shaken together for 72 h to allow saturation of both phases. Approximately 1 mg of the complexes was dissolved in 5 mL of the aqueous phase, and 5 mL of the organic phase was added, mixing for 10 min. The resulting emulsion was centrifuged to separate the phases. The concentration of the compounds in each phase was determined using UV−vis absorbance spectroscopy. log $D_{7.4}$ was defined as $\log\{[compound_{organic}]/[compound_{aqueous}]\}$.

4.5. Solution Chemistry. The stability of the gold complexes has been analyzed by absorption UV−vis spectroscopy and ^1H and $^{31}P\{^1H\}$ NMR spectroscopy.

UV−vis absorption spectra of the complexes were recorded on a Thermo Scientific spectrophotometer. Solutions of the thiolate complexes (5×10^{-5} M) in PBS (pH 7.4) were prepared from 20 mM DMSO stock solutions of the complexes and thereafter monitored by measuring the electronic spectra over 24 h at 37 °C.

A PBS solution (pH 7.4) was added to a DMSO-d_6 solution of the complexes in a 5:1 proportion (PBS/DMSO-d_6) and studied by NMR over a 24 h period. The signals in the region 4−5 ppm in the ^1H NMR spectrum disappeared as a result of the experimental procedure (pulse centered at 4.58 ppm).

4.6. Interaction with BSA. BSA was commercially available from Sigma-Aldrich. A 2 mM stock solution of BSA was prepared in PBS at pH 7.4. The real concentration was confirmed using UV−vis spectroscopy ($\varepsilon_{280\ nm}$ = 43824 M^{-1} cm^{-1}). Gold complexes were dissolved in DMSO to achieve 6 mM stock solutions, and six aliquots of 2.5 μL were added to a 50 μM solution of BSA in PBS, which was

DOI: 10.1021/acs.inorgchem.7b01370
Inorg. Chem. 2017, 56, 8562−8579

then placed in a quartz cuvette of 1 cm optical path. The final concentrations of the gold complexes in the cuvette were 0, 5, 10, 15, 20, 25, and 30 μM. The fluorescence spectra were recorded on a Jobin-Yvon-Horiba Fluorolog FL-3-11 spectrometer. The samples were excited at 295 nm, and the emission spectra were recorded in a range from 310 to 450 nm with emission slits set to 2 nm.

The samples were measured 240 s after every addition of the aliquots of gold complexes. The fluorescence intensities of PBS and the gold complexes were irrelevant under the described conditions, as were the effects of the addition of gold aliquots and of time incubation between measurements.

The data were analyzed using the Stern–Volmer equation $F_0/F = 1 + K_{SV}[\text{gold complex}] = 1 + K_q\tau_0[\text{gold complex}]$ in order to obtain the Stern–Volmer quenching constant (K_{SV}) and the quenching rate constant (K_q). The binding constant (K_b) was quantified by using the Stern–Volmer equation $\log\{(F_0 - F)/F\} = \log K_b + n \log [\text{gold complex}]$.

4.7. Growth Inhibition Assay. Human Caco-2 cell lines (PD7 and TC7 clones) were kindly provided by Dr. Edith Brot-Laroche (Université Pierre et Marie Curie-Paris 6, UMR S 872, Les Cordeliers, France). Caco-2 cells were maintained in a humidified atmosphere of 5% CO_2 at 37 °C. Cells (passages 50–80) were grown in Dulbecco's modified Eagle's medium (DMEM; Gibco Invitrogen, Paisley, U.K.), supplemented with 20% fetal bovine serum (FBS), 1% nonessential amino acids, 1% penicillin (1000 U mL^{-1}), 1% streptomycin (1000 μg mL^{-1}), and 1% amphotericin (250 μg mL^{-1}). Experiments were performed 24 h postseeding. Stock solutions of the complexes (saline solution or DMSO) were diluted in a complete medium to the required concentration. DMSO at similar concentrations did not show any effects on the cytotoxicity.

For cytotoxicity screening experiments, cells were seeded in 96-well plates at a density of 4×10^3 cells well^{-1}. The culture medium was replaced with a fresh medium (without FBS) containing the complexes at concentrations varying from 0 to 20 μM, with an exposure time of 72 h. In the cases of combinations of complexes **1**, **2**, **8**, and **9** with 5-FU, cells were treated with the mixture with total drug concentrations of 0, 1.25, 2.5, 5, 10, and 20 μM in a 1:1 ratio (e.g., 5 μM **2** + 5 μM 5-FU for a total drug concentration of 10 μM).

For cell viability studies of differentiated (enterocyte-like) cells, Caco-2/PD7 cells were seeded in 96-well plates at a density of 4×10^3 cells well^{-1} and incubated for approximately 10–15 days, with the culture medium changed every 3 days, up to confluence, the moment at which the cells were treated with the complexes at concentrations equal to their mean IC_{50} and 2 times the IC_{50} values.

Thereafter, cell survival was measured using the 3-(4,5-dimethyl-2-thiazoyl)-2,5-diphenyltetrazolium bromide (MTT, Merck) test as previously described.[16] The assay is dependent on the cellular reduction of MTT by the mitochondrial dehydrogenase of viable cells to a blue formazan product, which can be measured spectrophotometrically. Following appropriate incubation of the cells, with or without metallic complexes, MTT was added to each well in an amount equal to 10% of the culture volume, and gentle stirring in a gyratory shaker, which enhances dissolution and incubation, was continued at 37 °C for 4 h. Thereafter, the medium and MTT were removed, and DMSO was added to each well. At the end, the results were obtained by measuring the absorbance with a scanning multiwell spectrophotometer (BIOTEX SINERGY HT SIAFRTD) at a wavelength of 560/670 nm and compared to the values of control cells incubated in the absence of complexes. Experiments were conducted in quadruplicate wells and repeated at least three times.

4.8. CV. CV experiments were carried out in a standard three-electrode cell using a computerized Autolab potentiostat (PGSTAT 12, Autolab) controlled by *GPES* software (version 4.7). A glassy carbon electrode of 3 mm diameter was used as the working electrode. It was polished using alumina and a polishing pad after each measurement. A saturated calomel electrode (SCE) and a platinum wire were used as reference and counter electrodes, respectively. All of the experiments were carried out in Milli-Q water using a phosphate buffer (0.1 M, pH 7.4), which served as the supporting electrolyte as well. The complexes were added from a DMSO stock solution (50 mM, 2% v/v of DMSO in the final solution) to a concentration of 1 mM. Only [Au(SMe_2pyrim)(PTA-CH_2-*p*-NO_2-C_6H_4)]Br (**12**) precipitated in the aqueous solution. Each solution was deoxygenated by purging argon for 5 min. Potentials are reported versus SCE at room temperature and corrected from the background current.

4.9. Study of the Cell Death and Cell Cycle. Cell death and cell cycle analysis was performed in treated and nontreated Caco-2 cells and clones PD7 and TC7. Treated cells were incubated with complex **1** at a concentration equal to its IC_{50} (average value) for each one of the cell lines previously calculated for 72 h of treatment. Control cells were simply incubated with a maximal volume of DMSO added to the treated cells, always being lower than 0.05%, a concentration at which DMSO does not show cytotoxic effects. Analyses were performed at 24, 48, and 72 h.

4.10. Measurements of Apoptosis. After the appropriate incubation, cells were collected and stained with Annexin V-FTIC according to the manufacturer's instructions. A negative control was prepared containing unreacted cells in order to define the basal level of apoptotic and necrotic or dead cells. After incubation, cells were transferred to flow-cytometry tubes and washed twice with temperate PBS, suspended in 100 μL of annexinV binding buffer (10 mM Hepes/NaOH, pH 7.4, 140 mM NaCl, 2.5 mM $CaCl_2$), and then 5 μL of annexinV/fluorescein isothiocyanate and 5 μL of PI were added to each 100 μL of cell suspension. After incubation for 15 min at room temperature in the dark, 400 μL of 1X annexin binding buffer was added and analyzed by flow cytometry within 1 h. The signal intensity was measured using a FACSARIA BD and analyzed using a FASCDIVA BD.

4.11. Cell Cycle Analysis. After treatment, the cells were then fixed in 70% ice-cold ethanol and stored at 4 °C for 24 h. After centrifugation, the cells were rehydrated in PBS and stained with a PI (50 μg mL^{-1}) solution containing RNase A (100 μg mL^{-1}). PI-stained cells were analyzed for DNA content in a FACSARRAY BD equipped with an argon-ion laser. The red fluorescence emitted by PI was collected using a 620 nm longer pass filter as a measure of the amount of DNA-bound PI and displayed on a linear scale. The cell cycle distribution was determined on a linear scale. The percentage of cells in the cycle phases was determined using *MODIFIT 3.0* Verity software.

4.12. Analysis of the Combined Effects of 5-FU with Gold(I) Thiolates. The CI was used to study the synergic activity of the compounds,[100] and data were evaluated with the program developed by Chou et al.[101] The combinatory indexes were calculated by dividing the IC_{50} of the drugs in the combination by the IC_{50} of the individual drugs. The mathematical formula is as follows:

$$\text{CI} = \frac{\text{dose of 5-FU}}{IC_{50}(\text{5-FU})} + \frac{\text{dose of the gold complex}}{IC_{50}(\text{gold complex})}$$

In this formula, the sum of the doses of 5-FU and the corresponding gold complex leads to 50% growth inhibition of the cells. CI = 1 is indicative of an additive effect, CI < 1 indicates synergism, and CI > 1 indicates antagonism. The DRI values were also calculated by *CompuSyn* using the following formula (for 50% growth inhibition):

$$(\text{DRI})_{\text{5-FU}} = \frac{IC_{50}(\text{5-FU})}{\text{dose of 5-FU}}; (\text{DRI})_{\text{Au}} = \frac{IC_{50}(\text{gold complex})}{\text{dose of gold complex}}$$

where a DRI > 1 would show a reduction of the necessary dose, while DRI < 1 would indicate an increase of the needed concentration for the same effect.

4.13. Measurement of Intracellular ROS Generation. The production of ROS was measured in Caco-2/TC7 seeded at a 4000 cells well^{-1} concentration in a 96-well plate, as described above. After 24 h, the culture growth medium was removed, and the cells were washed with PBS 1X and incubated with 20 μM DCFH-DA (Sigma-Aldrich; 100 μL well^{-1}) at 37 °C for 45 min in the dark. Afterward, cells were washed with PBS 1X and then incubated with the tested compounds at their IC_{50} concentration or 500 μM H_2O_2 for the positive control. The fluorescent emission of DCF was monitored at

DOI: 10.1021/acs.inorgchem.7b01370
Inorg. Chem. 2017, 56, 8562–8579

530 nm right after the addition of the complexes for 3 h using a microplate reader (λ_{ex} = 485 nm), measuring every 15 min. The temperature was maintained at 37 °C during the experiment.

4.14. Determination of the Activity of Redox Enzymes. The method is based on the reaction of DTNB with thiol groups of proteins to form the 2-nitro-5-thiobenzoate anion (TNB^{2-}), which absorbs at λ_{max} = 412 nm.

For the in cellulo determination of the activity of redox enzymes, Caco-2/TC7 cells were seeded in a 96-well plate (4000 cells $well^{-1}$) and then treated with complex **1** (IC_{50} concentration) for 24 h. Cells were then lysed by adding 50 μL $well^{-1}$ of the lysis buffer [50 mM Tris-HCl + 2 mM ethylenediaminetetraacetic acid (EDTA), pH 7.5] for 20 min. The protein content was measured by the Bradford assay.[102] A total of 25 μL of the reaction mixture (for a total volume of 1 mL: 500 μL of PBS (1×), pH 7.0, 80 μL of 100 mM EDTA, pH 7.5, 20 μL of a 0.05% BSA solution, 100 μL of 20 mM NADPH, and 300 μL of Milli-Q water) was added, and the reaction was started by adding 25 μL of a 20 mM DTNB solution in methanol. The absorbance at 412 nm was monitored for 6 min. The activity of nontreated cells was considered as the control and estimated as 100% of the activity.

4.14.1. TrxR1 Activity Assay in Vitro. Recombinant human TrxR1 (Sigma SRP6081) was incubated in a 96-well plate with IC_{50} concentrations of auranofin, **1**, and **9** previously dissolved in 25 μL of PBS at pH 7.4. The cell solution was incubated in a shake motion for 75 min at 37 °C. After the incubation time, 25 μL of a reaction mixture (500 μL of PBS, pH 7, 80 μL of 100 mM EDTA, pH 7.5, 20 μL of 0.05% BSA, 100 μL of 20 mM NADPH, and 300 μL of distilled water) was added to each well. Finally, the reaction was started by adding 25 μL of 20 mM DNTB in pure ethanol. The absorbance at 412 nm was recorded each 10 s for 6 min as a measure of the TrxR activity.

■ ASSOCIATED CONTENT

Supporting Information

The Supporting Information is available free of charge on the ACS Publications website at DOI: 10.1021/acs.inorgchem.7b01370.

^{1}H, $^{31}P\{^{1}H\}$, $^{13}C\{^{1}H\}$, and HSQC NMR spectra of gold(I) complexes, UV−vis absorption spectra from stability assays, BSA fluorescence quenching spectra, cell viability (%) studies with enterocyte-like cells, absorbance values from cell viability, cell density plots from apoptosis assays, cyclic voltammograms, and ^{1}H and $^{31}P\{^{1}H\}$ NMR stability studies (PDF)

■ AUTHOR INFORMATION

Corresponding Authors

*E-mail: mlaguna@unizar.es.

*E-mail: ecerrada@unizar.es.

ORCID

Elena Cerrada: 0000-0003-2457-3674

Notes

The authors declare no competing financial interest.

■ ACKNOWLEDGMENTS

The authors thank Christelle Hureau (LCC, Toulouse, France) for use of the potentiostat to perform cyclic voltammetry measurements. We also thank Centro de Investigación Biomédica de Aragón for technical assistance (http://www.iacs.aragon.es), Servicio General de Apoyo a la Investigación, Universidad de Zaragoza, and S. A. Torrecid for a generous donation of $H[AuCl_4]$. E.C. and M.J.R.-Y. thank the Ministerio de Economia y Competitividad (Grants CTQ2016-75816-C2-1-P and SAF2016-75441-R, respectively) and DGA (Grants E104 and A-32) for financial support.

■ REFERENCES

(1) Ferlay, J.; Soerjomataram, I.; Ervik, M.; Dikshit, R.; Eser, S.; Mathers, C.; Rebelo, M.; Parkin, D. M.; Forman, D.; Bray, F. *GLOBOCAN 2012 v1.0: Cancer Incidence and Mortality Worldwide: IARC CancerBase No. 11 [online]*; International Agency for Research on Cancer: Lyon, France, 2013; http://globocan.iarc.fr.

(2) Andre, T.; Boni, C.; Mounedji-Boudiaf, L.; Navarro, M.; Tabernero, J.; Hickish, T.; Topham, C.; Zaninelli, M.; Clingan, P.; Bridgewater, J.; Tabah-Fisch, I.; de Gramont, A. Oxaliplatin, fluorouracil, and leucovorin as adjuvant treatment for colon cancer. *N. Engl. J. Med.* **2004**, *350*, 2343−2351.

(3) Andre, T.; Boni, C.; Navarro, M.; Tabernero, J.; Hickish, T.; Topham, C.; Bonetti, A.; Clingan, P.; Bridgewater, J.; Rivera, F.; de Gramont, A. Improved Overall Survival With Oxaliplatin, Fluorouracil, and Leucovorin As Adjuvant Treatment in Stage II or III Colon Cancer in the MOSAIC Trial. *J. Clin. Oncol.* **2009**, *27*, 3109−3116.

(4) Tournigand, C.; Andre, T.; Bonnetain, F.; Chibaudel, B.; Lledo, G.; Hickish, T.; Tabernero, J.; Boni, C.; Bachet, J.-B.; Teixeira, L.; de Gramont, A. Adjuvant Therapy With Fluorouracil and Oxaliplatin in Stage II and Elderly Patients (between ages 70 and 75 years) With Colon Cancer: Subgroup Analyses of the Multicenter International Study of Oxaliplatin, Fluorouracil, and Leucovorin in the Adjuvant Treatment of Colon Cancer Trial. *J. Clin. Oncol.* **2012**, *30*, 3353−3360.

(5) Andre, T.; de Gramont, A.; Vernerey, D.; Chibaudel, B.; Bonnetain, F.; Tijeras-Raballand, A.; Scriva, A.; Hickish, T.; Tabernero, J.; Van Laethem, J. L.; Banzi, M.; Maartense, E.; Shmueli, E.; Carlsson, G. U.; Scheithauer, W.; Papamichael, D.; Moeehler, M.; Landolfi, S.; Demetter, P.; Colote, S.; Tournigand, C.; Louvet, C.; Duval, A.; Flejou, J.-F.; de Gramont, A. Adjuvant Fluorouracil, Leucovorin, and Oxaliplatin in Stage II to III Colon Cancer: Updated 10-Year Survival and Outcomes According to BRAF Mutation and Mismatch Repair Status of the MOSAIC Study. *J. Clin. Oncol.* **2015**, *33*, 4176.

(6) Boulikas, T.; Vougiouka, M. Cisplatin and platinum drugs at the molecular level (review). *Oncol. Rep.* **2003**, *10*, 1663−1682.

(7) Raymond, E.; Faivre, S.; Chaney, S.; Woynarowski, J.; Cvitkovic, E. Cellular and molecular pharmacology of oxaliplatin. *Mol. Cancer Ther.* **2002**, *1*, 227−235.

(8) Falcone, A.; Ricci, S.; Brunetti, I.; Pfanner, E.; Allegrini, G.; Barbara, C.; Crino, L.; Benedetti, G.; Evangelista, W.; Fanchini, L.; Cortesi, E.; Picone, V.; Vitello, S.; Chiara, S.; Granetto, C.; Porcile, G.; Fioretto, L.; Orlandini, C.; Andreuccetti, M.; Masi, G. Phase III trial of infusional fluorouracil, leucovorin, oxaliplatin, and irinotecan (FOLFOXIRI) compared with infusional fluorouracil, leucovorin, and irinotecan (FOLFIRI) as first-line treatment for metastatic colorectal cancer: The Gruppo Oncologico Nord Ovest. *J. Clin. Oncol.* **2007**, *25*, 1670−1676.

(9) McWhinney, S. R.; Goldberg, R. M.; McLeod, H. L. Platinum neurotoxicity pharmacogenetics. *Mol. Cancer Ther.* **2009**, *8*, 10−16.

(10) Fries, J. F.; Bloch, D.; Spitz, P.; Mitchell, D. M. Cancer In Rheumatoid-Arthritis - A Prospective Long-Term Study Of Mortality. *Am. J. Med.* **1985**, *78*, 56−59.

(11) Mirabelli, C. K.; Johnson, R. K.; Sung, C.-M.; Faucette, L. F.; Murihead, K.; Crooke, S. T. Evaluation of the in vivo antitumor activity and in vitro cytotoxic properties of auranofin, a coordinated gold compound, in murine tumor models. *Cancer Res.* **1985**, *45*, 32−39.

(12) Madeira, J. M.; Gibson, D. L.; Kean, W. F.; Klegeris, A. The biological activity of auranofin: implications for novel treatment of diseases. *Inflammopharmacology* **2012**, *20*, 297−306.

(13) Berners-Price, S. J.; Filipovska, A. Gold compounds as therapeutic agents for human diseases. *Metallomics* **2011**, *3*, 863−873.

(14) Gasser, G.; Metzler-Nolte, N. The potential of organometallic complexes in medicinal chemistry. *Curr. Opin. Chem. Biol.* **2012**, *16*, 84−91.

(15) Gasser, G.; Ott, I.; Metzler-Nolte, N. Organometallic Anticancer Compounds. *J. Med. Chem.* **2011**, *54*, 3−25.

DOI: 10.1021/acs.inorgchem.7b01370
Inorg. Chem. 2017, 56, 8562−8579

(16) Bertrand, B.; Casini, A. A golden future in medicinal inorganic chemistry: the promise of anticancer gold organometallic compounds. *Dalton Trans.* **2014**, *43*, 4209−4219.
(17) Nardon, C.; Boscutti, G.; Fregona, D. Beyond Platinums: Gold Complexes as Anticancer Agents. *Anticancer Res.* **2014**, *34*, 487−492.
(18) Medici, S.; Peana, M.; Nurchi, V. M.; Lachowicz, J. I.; Crisponi, G.; Zoroddu, M. A. Noble metals in medicine: Latest advances. *Coord. Chem. Rev.* **2015**, *284*, 329−350.
(19) Ott, I. On the medicinal chemistry of gold complexes as anticancer drugs. *Coord. Chem. Rev.* **2009**, *253*, 1670−1681.
(20) Gutierrez, A.; Gracia-Fleta, L.; Marzo, I.; Cativiela, C.; Laguna, A.; Gimeno, M. C. Gold(I) thiolates containing amino acid moieties. Cytotoxicity and structure-activity relationship studies. *Dalton Trans.* **2014**, *43*, 17054−17066.
(21) CArlos Lima, J.; Rodriguez, L. Phosphine-Gold(I) Compounds as Anticancer Agents: General Description and Mechanisms of Action. *Anti-Cancer Agents Med. Chem.* **2011**, *11*, 921−928.
(22) Gutierrez, A.; Marzo, I.; Cativiela, C.; Laguna, A.; Gimeno, M. C. Highly Cytotoxic Bioconjugated Gold(I) Complexes with Cysteine-Containing Dipeptides. *Chem. - Eur. J.* **2015**, *21*, 11088−11095.
(23) Garcia-Moreno, E.; Gascon, S.; Atrian-Blasco, E.; Rodriguez-Yoldi, M. J.; Cerrada, E.; Laguna, M. Gold(I) complexes with alkylated PTA (1,3,5-triaza-7-phosphaadamantane) phosphanes as anticancer metallodrugs. *Eur. J. Med. Chem.* **2014**, *79*, 164−172.
(24) Miranda, S.; Vergara, E.; Mohr, F.; de Vos, D.; Cerrada, E.; Mendia, A.; Laguna, M. Synthesis, characterization, and in vitro cytotoxicity of some gold(I) and trans platinum(II) thionate complexes containing water-soluble PTA and DAPTA ligands. X-ray crystal structures of [Au(SC4H3N2)(PTA)], trans-[Pt(SC4H3N2)(2)(PTA)(2)], trans-[Pt(SC5H4N)(2)(PTA)(2)], and trans-[Pt-(SC5H4N)(2)(DAPTA)(2)]. *Inorg. Chem.* **2008**, *47*, 5641−5648.
(25) Vergara, E.; Cerrada, E.; Clavel, C.; Casini, A.; Laguna, M. Thiolato gold(I) complexes containing water-soluble phosphane ligands: a characterization of their chemical and biological properties. *Dalton Trans.* **2011**, *40*, 10927−10935.
(26) Vergara, E.; Casini, A.; Sorrentino, F.; Zava, O.; Cerrada, E.; Rigobello, M. P.; Bindoli, A.; Laguna, M.; Dyson, P. J. Anticancer Therapeutics That Target Selenoenzymes: Synthesis, Characterization, in vitro Cytotoxicity, and Thioredoxin Reductase Inhibition of a Series of Gold(I) Complexes Containing Hydrophilic Phosphine Ligands. *ChemMedChem* **2010**, *5*, 96−102.
(27) Keter, F. K.; Guzei, I. A.; Nell, M.; van Zyl, W. E.; Darkwa, J. Phosphinogold(I) Dithiocarbamate Complexes: Effect of the Nature of Phosphine Ligand on Anticancer Properties. *Inorg. Chem.* **2014**, *53*, 2058−2067.
(28) Gandin, V.; Fernandes, A. P.; Rigobello, M. P.; Dani, B.; Sorrentino, F.; Tisato, F.; Bjornstedt, M.; Bindoli, A.; Sturaro, A.; Rella, R.; Marzano, C. Cancer cell death induced by phosphine gold(I) compounds targeting thioredoxin reductase. *Biochem. Pharmacol.* **2010**, *79*, 90−101.
(29) de Vos, D.; Ho, S. Y.; Tiekink, E. R. T. Cytotoxicity profiles for a series of triorganophosphinegold(I) dithiocarbamates and triorganophosphinegold(I) xanthates. *Bioinorg. Chem. Appl.* **2004**, *2*, 141−154.
(30) Bhabak, K. P.; Bhuyan, B. J.; Mugesh, G. Bioinorganic and medicinal chemistry: aspects of gold(I)-protein complexes. *Dalton Trans.* **2011**, *40*, 2099−2111.
(31) McKeage, M. J.; Maharaj, L.; Berners-Price, S. J. Mechanisms of cytoxicity and antitumor activity og gold(I) phosphine complexes: the possible role of mitochondria. *Coord. Chem. Rev.* **2002**, *232*, 127−135.
(32) Bindoli, A.; Rigobello, M. P.; Scutari, G.; Gabbiani, C.; Casini, A.; Messori, L. Thioredoxin reductase: A target for gold compounds acting as potential anticancer drugs. *Coord. Chem. Rev.* **2009**, *253*, 1692−1707.
(33) Barnard, P. J.; Berners-Price, S. J. Targeting the mitochondrial cell death pathway with gold compounds. *Coord. Chem. Rev.* **2007**, *251*, 1889−1902.
(34) Saccoccia, F.; Angelucci, F.; Boumis, G.; Brunori, M.; Miele, A. E.; Williams, D. L.; Bellelli, A. On the mechanism and rate of gold incorporation into thiol-dependent flavoreductases. *J. Inorg. Biochem.* **2012**, *108*, 105−111.
(35) Gromer, S.; Arscott, L. D.; Williams, C. H.; Schirmer, R. H.; Becker, K. Human placenta thioredoxin reductase - Isolation of the selenoenzyme, steady state kinetics, and inhibition by therapeutic gold compounds. *J. Biol. Chem.* **1998**, *273*, 20096−20101.
(36) Baker, A.; Payne, C. M.; Briehl, M. M.; Powis, G. Thioredoxin, a gene found overexpressed in human cancer, inhibits apoptosis in vitro and in vivo. *Cancer Res.* **1997**, *57*, 5162−5167.
(37) Rundlof, A. K.; Arner, E. S. J. Regulation of the mammalian selenoprotein thioredoxin reductase 1 in relation to cellular phenotype, growth, and signaling events. *Antioxid. Redox Signaling* **2004**, *6*, 41−52.
(38) Hedstrom, E.; Eriksson, S.; Zawacka-Pankau, J.; Arner, E. S. J.; Selivanova, G. p53-dependent inhibition of TrxR1 contributes to the tumor-specific induction of apoptosis by RITA. *Cell Cycle* **2009**, *8*, 3584−3591.
(39) Nilsonne, G.; Sun, X.; Nystrom, C.; Rundlof, A. K.; Potamitou Fernandes, A.; Bjornstedt, M.; Dobra, K. Selenite induces apoptosis in sarcomatoid malignant mesothelioma cells through oxidative stress. *Free Radical Biol. Med.* **2006**, *41*, 874−885.
(40) Romero-Canelon, I.; Sadler, P. J. Next-Generation Metal Anticancer Complexes: Multitargeting via Redox Modulation. *Inorg. Chem.* **2013**, *52*, 12276−12291.
(41) García-Moreno, E.; Gascón, S.; Garcia de Jalón, J.; Romanos, E.; Rodriguez-Yoldi, M. J.; Cerrada, E.; Laguna, M. In vivo anticancer activity, toxicology and histopathological studies of the thiolate gold(I) complex [Au(Spyrimidine)(PTA-CH2Ph)]Br. *Anti-Cancer Agents Med. Chem.* **2015**, *15*, 773−782.
(42) García-Moreno, E.; Cerrada, E.; Bolsa, M. J.; Luquin, A.; Laguna, M. Water-Soluble Phosphanes Derived from 1,3,5-Triaza-7-phosphaadamantane and Their Reactivity towards Gold(I) Complexes. *Eur. J. Inorg. Chem.* **2013**, *2013*, 2020−2030.
(43) Miranda, S.; Vergara, E.; Mohr, F.; de Vos, D.; Cerrada, E.; Mendia, A.; Laguna, M. Synthesis, characterization, and in vitro cytotoxicity of some gold(I) and trans platinum(II) thionate complexes containing water-soluble PTA and DAPTA ligands. X-ray crystal structures of Au(SC4H3N2)(PTA), trans- Pt(SC4H3N2)(2)(PTA)(2), trans- Pt(SC5H4N)(2)(PTA)(2), and trans- Pt-(SC5H4N)(2)(DAPTA)(2). *Inorg. Chem.* **2008**, *47*, 5641−5648.
(44) Atrián-Blasco, E.; Gascón, S.; Rodríguez-Yoldi, M. J.; Laguna, M.; Cerrada, E. Synthesis of Gold(I) Derivatives Bearing Alkylated 1,3,5-Triaza-7-phosphaadamantane as Selective Anticancer Metallodrugs. *Eur. J. Inorg. Chem.* **2016**, *2016*, 2791−2803.
(45) Jia, G.; Puddephatt, R. J.; Vittal, J. J. Gold complexes and polymers with pyridinethiols: The crystal and molecular structure of [AuCl(pyridinium-2-thione)]. *Polyhedron* **1992**, *11*, 2009−2014.
(46) Kerns, E. H.; Di, L. *Drug-like properties: concepts, structure design and methods: from ADME to toxicity optimization*; Elsevier: New York, 2008.
(47) Lombardo, F.; Obach, R. S.; Shalaeva, M. Y.; Gao, F. Prediction of volume of distribution values in humans for neutral and basic drugs using physicochemical measurements and plasma protein binding data. *J. Med. Chem.* **2002**, *45*, 2867−2876.
(48) Fonteh, P.; Elkhadir, A.; Omondi, B.; Guzei, I.; Darkwa, J.; Meyer, D. Impedance technology reveals correlations between cytotoxicity and lipophilicity of mono and bimetallic phosphine complexes. *BioMetals* **2015**, *28*, 653−667.
(49) Santini, C.; Pellei, M.; Papini, G.; Morresi, B.; Galassi, R.; Ricci, S.; Tisato, F.; Porchia, M.; Rigobello, M. P.; Gandin, V.; Marzano, C. In vitro antitumour activity of water soluble Cu(I), Ag(I) and Au(I) complexes supported by hydrophilic alkyl phosphine ligands. *J. Inorg. Biochem.* **2011**, *105*, 232−240.
(50) Liu, J. J.; Galettis, P.; Farr, A.; Maharaj, L.; Samarasinha, H.; McGechan, A. C.; Baguley, B. C.; Bowen, R. J.; Berners-Price, S. J.; McKeage, M. J. In vitro antiturnour and hepatotoxicity profiles of Au(I) and Ag(I) bidentate pyridyl phosphine complexes and relationships to cellular uptake. *J. Inorg. Biochem.* **2008**, *102*, 303−310.
(51) McKeage, M. J.; Berners-Price, S. J.; Galettis, P.; Bowen, R. J.; Brouwer, W.; Ding, L.; Zhuang, L.; Baguley, B. C. Role of lipophilicity

DOI: 10.1021/acs.inorgchem.7b01370
Inorg. Chem. 2017, 56, 8562−8579

in determining cellular uptake and antitumour activity of gold phosphine complexes. *Cancer Chemother. Pharmacol.* **2000**, *46*, 343−350.
(52) Berners-Price, S. J.; Filipovska, A. The design of gold-based, mitochondria-targeted chemotherapeutics. *Aust. J. Chem.* **2008**, *61*, 661−668.
(53) Garcia-Moreno, E.; Gascon, S.; Rodriguez-Yoldi, M. J.; Cerrada, E.; Laguna, M. S-Propargylthiopyridine Phosphane Derivatives As Anticancer Agents: Characterization and Antitumor Activity. *Organometallics* **2013**, *32*, 3710−3720.
(54) Sánchez-de-Diego, C.; Mármol, I.; Pérez, R.; Gascón, S.; Rodriguez-Yoldi, M. J.; Cerrada, E. The anticancer effect related to disturbances in redox balance on Caco-2 cells caused by an alkynyl gold(I) complex. *J. Inorg. Biochem.* **2017**, *166*, 108−121.
(55) Cheng, A. L.; Merz, K. M. Prediction of aqueous solubility of a diverse set of compounds using quantitative structure-property relationships. *J. Med. Chem.* **2003**, *46*, 3572−3580.
(56) Di, L.; Kerns, E. H.; Chen, H.; Petusky, S. L. Development and application of an automated solution stability assay for drug discovery. *J. Biomol. Screening* **2006**, *11*, 40−7.
(57) Kerns, E. H.; Di, L., Chemical Stability. *Comprehensive medicinal chemistry*; Elsevier: Philadelphia, PA, 2006; Vol. *5*, pp 489−507.
(58) Vogler, A.; Kunkely, H. Photoreactivity of gold complexes. *Coord. Chem. Rev.* **2001**, *219−221*, 489−507.
(59) Nobili, S.; Mini, E.; Landini, I.; Gabbiani, C.; Casini, A.; Messori, L. Gold compounds as anticancer agents: chemistry, cellular pharmacology, and preclinical studies. *Med. Res. Rev.* **2009**, *30*, 550−580.
(60) Ascenzi, P.; Bocedi, A.; Notari, S.; Fanali, G.; Fesce, R.; Fasano, M. Allosteric modulation of drug binding to human serum albumin. *Mini-Rev. Med. Chem.* **2006**, *6*, 483−489.
(61) Roberts, J. R.; Xiao, J.; Schliesman, B.; Parsons, D. J.; Shaw, C. F. Kinetics and mechanism of the reaction between serum albumin and auranofin (and its isopropyl analogue) in vitro. *Inorg. Chem.* **1996**, *35*, 424−433.
(62) Christodoulou, J.; Sadler, P. J.; Tucker, A. A new structural transition of serum-albumin dependent on the state of cys34 - detection by h-1-nmr spectroscopy. *Eur. J. Biochem.* **1994**, *225*, 363−368.
(63) Mirabelli, C. K.; Johnson, R. K.; Sung, C. M.; Faucette, L.; Muirhead, K.; Crooke, S. T. Evaluation of the invivo antitumor-activity and invitro cyto-toxic properties of auranofin, a coordinated gold compound, in murine tumor-models. *Cancer Res.* **1985**, *45*, 32−39.
(64) Carter, D.; Ho, J. X. *Advances in Protein Chemistry*; Academic Press: New York, 1994; Vol. *45*.
(65) Peters, T. J. Serum Albumin. *Adv. Protein Chem.* **1985**, *37*, 161−245.
(66) Lakowicz, J. R. *Principles of Fluorescence Spectroscopy*; Springer: Baltimore, MD, 2006; pp 277−330.
(67) Sanghvi, C. D.; Olsen, P. M.; Elix, C.; Peng, S.; Wang, D. S.; Chen, Z.; Shin, D. M.; Hardcastle, K. I.; MacBeth, C. E.; Eichler, J. F. Antitumor properties of five-coordinate gold(III) complexes bearing substituted polypyridyl ligands. *J. Inorg. Biochem.* **2013**, *128*, 68−76.
(68) Canumalla, A. J.; Schraa, S.; Isab, A. A.; Shaw, C. F., III; Gleichmann, E.; Dunemann, L.; Turfeld, M. Equilibrium binding constants and facile dissociation of novel serum albumin-dicyanoaurate(I) complexes. *JBIC, J. Biol. Inorg. Chem.* **1998**, *3*, 9−17.
(69) Garcia-Moreno, E.; Tomas, A.; Atrian-Blasco, E.; Gascon, S.; Romanos, E.; Rodriguez-Yoldi, M. J.; Cerrada, E.; Laguna, M. In vitro and in vivo evaluation of organometallic gold(I) derivatives as anticancer agents. *Dalton Trans.* **2016**, *45*, 2462−2475.
(70) Neault, J. F.; Tajmir-Riahi, H. A. Interaction of cisplatin with human serum albumin. Drug binding mode and protein secondary structure. *Biochim. Biophys. Acta, Protein Struct. Mol. Enzymol.* **1998**, *1384*, 153−159.
(71) Yue, H. L.; Hu, Y. J.; Chen, J.; Bai, A. M.; Ouyang, Y. Green synthesis and physical characterization of Au nanoparticles and their interaction with bovine serum albumin. *Colloids Surf., B* **2014**, *122*, 107−114.
(72) Zheng, C. Z.; Wang, H. P.; Xu, W.; Xu, C. Y.; Liang, J. G.; Han, H. Y. Study on the interaction between histidine-capped Au nanoclusters and bovine serum albumin with spectroscopic techniques. *Spectrochim. Acta, Part A* **2014**, *118*, 897−902.
(73) Rousset, M. The human colon carcinoma cell lines HT-29 and Caco-2: Two in vitro models for the study of intestinal differentiation. *Biochimie* **1986**, *68*, 1035−1040.
(74) Meunier, V.; Bourrie, M.; Berger, Y.; Fabre, G. The human intestinal epithelial-cell line caco-2 - pharmacological and pharmacokinetic applications. *Cell Biol. Toxicol.* **1995**, *11*, 187−194.
(75) Chantret, I.; Rodolosse, A.; Barbat, A.; Dussaulx, E.; Brotlaroche, E.; Zweibaum, A.; Rousset, M. Differential Expression Of Sucrase-Isomaltase In Clones Isolated From Early And Late Passages Of The Cell-Line Caco-2 - Evidence For Glucose-Dependent Negative Regulation. *J. Cell. Sci.* **1994**, *107*, 213−225.
(76) Mosmann, T. Rapid colorimetric assay for cellular growth and survival - application to proliferation and cyto-toxicity assays. *J. Immunol. Methods* **1983**, *65*, 55−63.
(77) Koelle, U.; Laguna, A. Electrochemistry of Au-complexes. *Inorg. Chim. Acta* **1999**, *290*, 44−50.
(78) Mohamed, A. A.; Bruce, A. E.; Bruce, A. M. R. Cyclic Voltammetry of Auranofin. *Metal-Based Drugs* **1999**, *6*, 233−238.
(79) Zweibaum, A.; Bourel, M.; Lestradet, H.; Chretien, J.; Richet, G. Differentiation of human colon-cancer cells - a new approach of colon-cancer. *Bull. Acad. Natl. Med.* **1993**, *177*, 63−73.
(80) Graham, J. S. C. J. Adjuvant therapy in colon cancer. *Expert Rev. Anticancer Ther.* **2012**, *12*, 99−109.
(81) Chou, T. C.; Talalay, P. Quantitative-analysis of dose-effect relationships - the combined effects of multiple-drugs or enzyme-inhibitors. *Adv. Enzyme Regul.* **1984**, *22*, 27−55.
(82) Kaufmann, S. H.; Earnshaw, W. C. Induction of Apoptosis by Cancer Chemotherapy. *Exp. Cell Res.* **2000**, *256*, 42−49.
(83) Nicholson, D. W. From bench to clinic with apoptosis-based therapeutic agents. *Nature* **2000**, *407*, 810−816.
(84) Trachootham, D.; Alexandre, J.; Huang, P. Targeting cancer cells by ROS-mediated mechanisms: a radical therapeutic approach? *Nat. Rev. Drug Discovery* **2009**, *8*, 579−591.
(85) Jungwirth, U. K. C. R.; Kowol, C. R.; Keppler, B. K.; Hartinger, C. G.; Berger, W.; Heffeter, P. Anticancer activity of metal complexes: Involvement of redox processes. *Antioxid. Redox Signaling* **2011**, *15*, 1085−1127.
(86) Cheng, X. L.; Holenya, P.; Can, S.; Alborzinia, H.; Rubbiani, R.; Ott, I.; Wolfl, S. A TrxR inhibiting gold(I) NHC complex induces apoptosis through ASK1-p38-MAPK signaling in pancreatic cancer cells. *Mol. Cancer* **2014**, *13*, 221.
(87) Holmgren, A. L. M.; Luthman, M. Tissue distribution and subcellular localization of bovine thioredoxin determined by radio-immunoassay. *Biochemistry* **1978**, *17*, 4071−4077.
(88) Karlenius, T. C.; Tonissen, K. F. Thioredoxin and Cancer: A Role for Thioredoxin in all States of Tumor Oxygenation. *Cancers* **2010**, *2*, 209−232.
(89) Urig, S.; Becker, K. On the potential of thioredoxin reductase inhibitors for cancer therapy. *Semin. Cancer Biol.* **2006**, *16*, 452−465.
(90) Marzano, C.; Gandin, V.; Folda, A.; Scutari, G.; Bindoli, A.; Rigobello, M. P. Inhibition of thioredoxin reductase by auranofin induces apoptosis in cisplatin-resistant human ovarian cancer cells. *Free Radical Biol. Med.* **2007**, *42*, 872−881.
(91) Pia Rigobello, M.; Messori, L.; Marcon, G.; Agostina Cinellu, M.; Bragadin, M.; Folda, A.; Scutari, G.; Bindoli, A. Gold complexes inhibit mitochondrial thioredoxin reductase: consequences on mitochondrial functions. *J. Inorg. Biochem.* **2004**, *98*, 1634−1641.
(92) Saccoccia, F. A.; Angelucci, F.; Boumis, F.; Carotti, G.; Desiato, D.; Miele, G.; Bellelli, A. E. Thioredoxin Reductase and its Inhibitors. *Curr. Protein Pept. Sci.* **2014**, *15*, 621−646.
(93) Saccoccia, F.; Angelucci, F.; Boumis, G.; Carotti, D.; Desiato, G.; Miele, A. E.; Bellelli, A. Thioredoxin Reductase and its Inhibitors. *Curr. Protein Pept. Sci.* **2014**, *15*, 621−646.
(94) Illan-Cabeza, N. A. G.-G.; Garcia-Garcia, A. R.; Martinez-Martos, J. M.; Ramirez-Exposito, M. J.; Pena-Ruiz, T.; Moreno-

DOI: 10.1021/acs.inorgchem.7b01370
Inorg. Chem. 2017, 56, 8562−8579

Carretero, M. N. A potential antitumor agent, (6-amino-1-methyl-5-nitrosouracilato-N3)-triphenylphosphine-gold(I): Structural studies and in vivo biological effects against experimental glioma. *Eur. J. Med. Chem.* **2013**, *64*, 260−272.
(95) Garcia, A.; Machado, R. C.; Grazul, R. M.; Lopes, M. T. P.; Correa, C. C.; Dos Santos, H. F.; de Almeida, M. V.; Silva, H. Novel antitumor adamantane-azole gold(I) complexes as potential inhibitors of thioredoxin reductase. *JBIC, J. Biol. Inorg. Chem.* **2016**, *21*, 275−292.
(96) Ortego, L.; Cardoso, F.; Martins, S.; Fillat, M. F.; Laguna, A.; Meireles, M.; Villacampa, M. D.; Gimeno, M. C. Strong inhibition of thioredoxin reductase by highly cytotoxic gold(I) complexes. DNA binding studies. *J. Inorg. Biochem.* **2014**, *130*, 32−37.
(97) Schuh, E.; Pfluger, C.; Citta, A.; Folda, A.; Rigobello, M. P.; Bindoli, A.; Casini, A.; Mohr, F. Gold(I) Carbene Complexes Causing Thioredoxin 1 and Thioredoxin 2 Oxidation as Potential Anticancer Agents. *J. Med. Chem.* **2012**, *55*, 5518−5528.
(98) Uson, R.; Laguna, A.; Laguna, M.; Briggs, D. A.; Murray, H. H.; Fackler, J. P. Tetrahydrothiophene gold(I) or gold(III) complexes. *Inorg. Synth.* **1989**, *26*, 85−91.
(99) Wetzel, C.; Kunz, P. C.; Kassack, M. U.; Hamacher, A.; Böhler, P.; Watjen, W.; Ott, I.; Rubbiani, R.; Spingler, B. *Dalton Trans.* **2011**, *40*, 9212−9220.
(100) Chou, T.; Talalay, P. Quantitative analysis of dose-effect relationships: the combined effects of multiple drugs or enzyme inhibitors. *Adv. Enzyme Regul.* **1984**, *22*, 27−55.
(101) Chou, T. C.; Martin, N. *CompuSyn software for drug combinations and for general dose-effect analysis, and user's guide* (www.combosyn.com), 2007.
(102) Bradford, M. M. A rapid and sensitive method for the quantitation of microgram quantities of protein utilizing the principle of protein-dye binding. *Anal. Biochem.* **1976**, *72*, 248−254.

DOI: 10.1021/acs.inorgchem.7b01370
Inorg. Chem. 2017, 56, 8562−8579